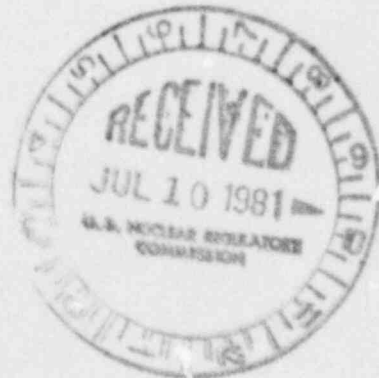



NUREG/CR-2103
UCRL-53020

Scaling and Estimation of Earthquake Ground Motion as a Function of the Earthquake Source Parameters and Distance

D. L. Bernreuter

Prepared for
U.S. Nuclear Regulatory Commission



 **LAWRENCE
LIVERMORE
LABORATORY**

8107140205 810630
PDR NUREG
CR-2103 R PDR

NOTICE

This report was prepared as an account of work sponsored by an agency of the United States Government. Neither the United States Government nor any agency thereof, or any of their employees, makes any warranty, expressed or implied, or assumes any legal liability or responsibility for any third party's use, or the results of such use, of any information, apparatus product or process disclosed in this report, or represents that its use by such third party would not infringe privately owned rights.

Available from

GPO Sales Program
Division of Technical Information and Document Control
U. S. Nuclear Regulatory Commission
Washington, D. C. 20555

Printed copy price: \$4.25

and

National Technical Information Service
Springfield, Virginia 22161

NUREG/CR-2103
UCRL-53020
RD

Scaling and Estimation of Earthquake Ground Motion as a Function of the Earthquake Source Parameters and Distance

Manuscript Completed: April 1981
Date Published: June 1981

Prepared by
D. L. Bernreuter

**Lawrence Livermore Laboratory
7000 East Avenue
Livermore, CA 94550**

**Prepared for
Office of Nuclear Regulatory Research
U.S. Nuclear Regulatory Commission
Washington, D.C. 20555
NRC FIN No. No. A0223**

ABSTRACT

In this report we review the various methodologies currently available to predict the near-source ground motion from an earthquake. The limitations of the various approaches are discussed in light of recently developed theory and recorded data. To overcome some of the limitations of available approaches, we develop improved rules for scaling between earthquakes. Ground-motion data obtained from salvo (line source) explosions are also investigated to gain insight into the appropriate form for the attenuation of peak acceleration and peak velocity. The scaling laws are combined with the appropriate attenuation relations and the data from the 1971 San Fernando and 1940 Imperial Valley earthquakes to obtain relations among the key source parameters: dynamic stress drop and equivalent radius of the highly stressed region, distance from the center of energy release, and peak ground acceleration and velocity. These relations are verified by comparing the predicted levels of ground motion to those actually recorded from a number of earthquakes, including the recent 1979 Imperial Valley and Coyote Lake earthquakes. The relations among earthquake magnitude, earthquake source parameters, and peak ground motion are discussed.

CONTENTS

Abstract	111
List of illustrations	vii
List of Tables	x
Executive Summary	1
Introduction	3
Assessment of Various Approaches	4
Quasi-Baysian Approaches	6
Regression Analysis Approaches	13
Simple Modeling	17
Computational Approaches	22
Scaling Rules	23
Attenuation	29
Basic Equations and Verification	32
The Role of Magnitude	59
Discussion of Results	63
Conclusions	66
References	67

LIST OF ILLUSTRATIONS

1. Peak acceleration vs. distance for earthquakes of various magnitudes	7
2. Estimated relationship between peak acceleration and distance from source for magnitude-6.5 earthquakes	8
3. Ranges of maximum acceleration in rock (Schnabel and Seed)	12
4. Comparison of correlations between epicentral distance and peak acceleration obtained by Trifunac to those of McGuire and Donovan for $M_L = 4.5$ and 6.5	14
5. Comparison of Ambraseys's correlation of epicentral distance and peak acceleration for Europe to those of Trifunac and McGuire for $M_L = 5.0$	16
6. Simplified model of a fault zone with region of high dynamic stress, used to develop scaling rules	24
7. Comparison of scaled peak acceleration from a number of explosions of different sizes	28
8. Attenuation of peak ground velocity, "Boxcar" explosion	30
9. Attenuation of peak ground velocity, "Danny Boy" explosion (0.43 kt, single device)	31
10. Attenuation of peak ground velocity, "Dugout" explosion--salvo of five 0.02-kt devices, line source of 0.55 km (180 ft)	32
11. Attenuation of peak ground velocity, "Buggy" explosion--salvo of five 1.1-kt devices, line source of 0.18 km (590 ft)	32
12. Attenuation of peak ground velocity, "Pre-Gondola II" explosion--salvo of five charges, $L = 0.1$ km (320 ft)	33
13. Attenuation of peak ground velocity, "Dip IIA" explosion-- $L = 0.07$ km (200 ft); 0.04 kt	33
14. Longitudinal centerline peak velocities, "Dip VA" explosion-- $L = 0.38$ km (1136 ft); 0.04 kt	34
15. Fit of San Fernando earthquake data (Table 4) to Eq. (17) using parameters in Table 6	37
16. Fit of May 1940 El Centro earthquake data (Table 5) to Eq. (17) using parameters in Table 6	37

17.	Combined fit of San Fernando and El Centro earthquake data to Eq. (17); scaled using $\rho_o = 1.0$ (rock), $\rho_o = 0.67$ (soil), and parameters in Table 6	38
18.	Fit of Eq. (22) to Fourier amplitude spectra of acceleration, various earthquakes	41
19.	Fit of Eq. (22) to Fourier amplitude spectra of acceleration, Parkfield and San Fernando earthquakes	42
20.	Fit of Eq. (22) to Fourier amplitude spectra of acceleration, Imperial Valley and Gilroy earthquakes	43
21.	Fit of Eq. (21) to the acceleration recorded for the Lytle Creek earthquake	44
22.	Fit of Eq. (21) to data from the Borrego Mountain earthquake	44
23.	Fit of Eq. (21) to the recorded peak acceleration for the 1952 Kern County earthquake	45
24.	Fit of Eq. (21) to data from the 1957 San Francisco earthquake	45
25.	Fit of Eq. (21) to data from the Parkfield earthquake, using two different locations for the region of high stress drop	46
26.	Fit of Eq. (21) to the recorded peak acceleration for the San Fernando earthquake (data from rock sites only)	47
27.	Fit of Eq. (21) to data from the October 1979 Imperial Valley earthquake, El Centro array	47
28.	Fit of Eq. (21) to data from the August 1979 Coyote Lake earthquake	47
29.	San Andreas fault near Parkfield, showing recording stations and trace fault	48
30.	Strong-motion stations in the Imperial Valley, California	51
31.	Postulated arrival times of S wave at selected stations of the El Centro array	53
32.	Location of the epicenter of the Coyote Lake earthquake, main shock and aftershocks	56
33.	Fit of Eq. (25) to the peak velocity recorded for the San Fernando earthquake	58

34.	Fit of Eq. (25) to the data recorded from the Lytle Creek earthquake	58
35.	Fit of Eq. (25) to the data recorded from the Borrego Mountain earthquake	59
36.	Fit of Eq. (25) to the peak velocity recorded at the El Centro array, Imperial Valley earthquake, October 15, 1979	59
37.	Estimated peak g value of earthquakes of various magnitudes for two values of stress drop	65

LIST OF TABLES

1.	Near-fault horizontal ground acceleration	11
2.	Typical results of regression analysis	15
3.	Earthquake-related data, salvo explosions	31
4.	Source parameters calculated by Trifunac for the San Fernando earthquake and initial aftershock	35
5.	Source parameters calculated by Trifunac for the El Centro earthquake and initial aftershock	36
6.	Coefficients A^* and n in Eq. (17) obtained by a least-squares fit to data in Tables 4 and 5	36
7.	Earthquakes used to verify Eqs. (21) and (25) and the source parameters obtained via a fit of Brune's model to selected Fourier spectra from strong-motion accelerograph data	39
8.	Arrival times of S wave at stations of the El Centro array, distances, and peak ground motion	52

EXECUTIVE SUMMARY

The problem of specifying the design ground motion produced by nearby earthquakes is not a new one, and a number of different approaches have been developed. In this paper we examine the most generally used approaches in the light of special requirements for specifying the design ground motion for nuclear power plants, recent developments in seismology, and recently acquired strong-ground-motion data. We conclude that the available methods are not very satisfactory and that an improved methodology is needed. Two key earthquake source parameters are identified: dynamic stress drop and equivalent radius of the high-stress zone.

To develop an improved methodology to predict the ground motion from an earthquake, we derive scaling rules to enable the comparison of ground motion from earthquakes with different source parameters. We also develop appropriate attenuation relations for strong ground motion by using both explosion and earthquake data. The data from salvo-type (line source) explosions are very useful, as measurements exist from the very near source to the very far field. The attenuation model and scaling rules are combined to obtain estimates of the peak ground acceleration and velocity as a function of the key earthquake source parameters and distance. These are verified by comparison with recorded data from a number of earthquakes, including the 1979 Imperial Valley and Coyote Lake earthquakes.

Many of the conclusions of this report are not new; however, the scaling rules and estimates of peak ground acceleration and velocity provide a way to relate the ground motion from various earthquakes. The results do underscore the conclusion that the energy released from a rupturing fault is highly variable, and that to understand the ground motion recorded at any particular station it is necessary to use the correct distance from the center of the zone of maximum high-frequency energy release near the station and not to approximate this by using the shortest distance to the fault. A few kilometers difference introduces significant differences in ground motion, particularly in the near-source region.

Our results can be used to make estimates of the ground motion very near the fault; however, when $r/L < 1$, where r is the distance from the center of localized faulting and L is the equivalent fault radius, our equations give estimates that are too high. We found that the parameter L is sufficiently

small and the center of local energy release sufficiently deep so that our equations are generally valid to within a few kilometers of the fault.

The scaling rules and equations we develop are based on simplistic concepts, and provide only a first approximation to the ground motion that can be expected from an earthquake with a given location and estimated ranges for the key source parameters $\Delta\sigma$ and L . Corrections should be applied to the estimates to account for any significant site factors and any potential for the seismic energy focusing towards the site.

The relations among earthquake magnitude, peak ground motion, and the key earthquake source parameters of stress drop and equivalent radius are examined, and very approximate relations are developed.

Our results show that peak acceleration is a function of both earthquake magnitude and stress drop, while peak velocity is much more than just a function of an earthquake's magnitude.

INTRODUCTION

One of the most important steps in the seismic design process is to specify the appropriate ground motion to be input into the design analysis. From the point of view of engineering design analysis, the important parameters are peak ground acceleration, spectral shape, and peak spectral levels. An earthquake is usually specified by giving its magnitude and either the epicentral distance or the distance of the closest point on the causative fault to the site.

The task of predicting the design ground motion at a given site for a critical facility, such as a nuclear power plant, is difficult because remote events (those having long return periods) must be considered in the analysis. It is often difficult even to specify the "strength" and location of the earthquake that governs the seismic design. In addition, earthquakes located nearby often become an important consideration. For example, even with the careful and detailed site investigations conducted at the Diablo Canyon Nuclear Power Plant site in California, a major nearby fault was discovered after the facility was nearly completed.

The task of specifying the design ground motion from nearby earthquakes is difficult because:

1. Magnitude is not the best parameter to use to define the "strength" of an earthquake.¹
2. Few near-source data are available to establish the appropriate form for the attenuation of the ground motion with distance, source size, and "strength."²⁻⁵
3. The available data are restricted to a few regions of high seismicity, and it is known that the attenuation in other regions can be significantly different.^{6,7}

The problem of specifying the ground motion for design purposes is not new, and a number of different approaches have been developed. In this paper we examine the most generally used approaches in light of special requirements for specifying the design ground motion for nuclear power plants, recent developments in seismology, and recently acquired data on strong ground motion. The latter part of this report deals with the proper scaling laws for different earthquakes and the conditions under which scaling is possible. This report attempts to shed some light on the question of how the ground motions

of different earthquakes of the same magnitude are related and the difficulty of relating ground-motion parameters such as peak acceleration to earthquake magnitude close to an earthquake.

In this report we use the term "near source" to mean earthquake ground motion recorded within 20 km of a fault, "far field" for distances greater than 200 km, and "intermediate field" for the range $20 \leq r \leq 200$.

ASSESSMENT OF VARIOUS APPROACHES

The various approaches to the specification of the ground motion can be conveniently lumped into the following categories:

1. Quasi-Baysian - All of the approaches that derive results based to a large extent on judgment rather than the direct outcome of a regression analysis.
2. Regression Analysis - All of the approaches that relate the ground motion parameters to earthquake specification and location obtained via a regression analysis using subsets of the available data.
3. Simple Modeling - All of the methods that derive results from an examination of the basic equations of motion and extremely simplified physics without resorting to the complex modeling and calculational effort required in Item 4.
4. Calculational - All of the approaches that make use of finite difference and finite-element methods of analysis and attempt to model the physics of the faulting process.

The two categories we have labeled Quasi-Baysian and Regression Analysis have much in common, in that both use the basic data to obtain empirical relations among earthquake magnitude, epicentral distance, and various ground-motion parameters. In the Regression Analysis category, we lump all those studies that derive their final relations via strict statistical analysis (e.g., Refs. 2, 8-19). In the Quasi-Baysian category we have lumped those approaches that use subsets of the data and obtain relations via "eyeball" fits and the use of various correction factors derived from the introduction of certain assumptions and models (e.g., Refs. 20-31). In some cases, both approaches are used; e.g., Trifunac² used a strict regression analysis approach to obtain relations among the ground motion, epicentral distance,

site conditions, and earthquake magnitude. However, in order to make estimates in the near field, he resorted to introducing Brune's model,³² other data, complex analysis, and considerable judgment.

Only recently have sufficient data become available to carry out a meaningful statistical analysis. Thus all of the pre-1970 approaches fall in the Quasi-Baysian category. In either case, the magnitude of the earthquake plays a central role; i.e., it is assumed that peak ground motion correlates directly with magnitude. This is the same as assuming that all earthquakes are dynamically similar and that the only similarity parameter needed to scale between events is magnitude. (We show in later sections that at least two parameters are required to scale between earthquakes.)

It must be kept in mind that the magnitude scale was arrived at by empirical considerations^{22,23} and, as it turns out, is the most difficult parameter to relate theoretically to other important source parameters (e.g., fault offset, stress drop, source dimension, seismic moment, and radiated seismic energy). A number of magnitude scales are commonly used; e.g., Richter local magnitude, body-wave magnitude, and surface-wave magnitude. These scales are not directly related and give different values; thus considerable care must be taken to note the scale used to measure the magnitude.³³ In addition, the Richter Scale is a regional empirical scale; hence, magnitudes determined in regions other than southern California using this scale are not necessarily the same measure of earthquake strength. Also, the magnitude is typically determined from band-limited seismometers at far-field distances of hundreds to thousands of kilometers, and gives little indication of the near-source strong ground motion. Even with these limitations the magnitude of an earthquake is still the most widely used measure of an earthquake's strength. Typically, the variation among the scales or among different stations reporting an M_L is about 0.5 or more units, and this leads to about a 50 percent change in the resultant acceleration. Thus the question of the measure of earthquake strength used is not a trivial one. This makes it somewhat difficult to intermix data from various areas. This should be done only with considerable care.

The fact that the magnitude of an earthquake may not completely specify the scaling between earthquakes can be partly incorporated into the Regression Analysis approach by computing the standard deviation and/or including confidence limits.^{2,9,14} Such an approach would be acceptable if we had an

adequate data base. This is not the case, as most of the data come from southern California and many are from a single earthquake.^{2,3,9,14}

Typically, nuclear power plants will not be located in highly seismic regions, yet the available data are from such regions. Thus it is not known whether the statistics are meaningful when a site is located in a region whose seismic characteristics are much different from California's. For example, it is well known that earthquakes with similar energy release (as measured by the surface-wave magnitude) are felt over an area a factor of ten or so larger in the eastern United States as compared to California.^{6,7} Another possible example is the large difference in the relation between intensity and acceleration in Europe and in the United States.^{16,34}

Figure 1 gives some recently recorded peak accelerations for a number of both large and small earthquakes. These data are taken from a number of sources, including Ref. 26. One important feature of the figure is that large accelerations have been recorded from small as well as large earthquakes. For later comparisons with various correlations, it is also important to note the large variation of ground motion within a limited magnitude range.

QUASI-BAYSIAN APPROACHES

Quasi-Baysian methods typically fall into several basic subcategories. For example, Gutenberg and Richter,^{22,23} Hofmann,²⁴ Housner,²⁵ and Page et al.²⁶ use the basic data and insight to obtain the required relations among peak ground motion, distance, and earthquake magnitude. Others, such as Kanai,²⁷ Seed and his co-workers,²⁸⁻³¹ and Blum,²¹ introduce corrections based on transfer functions derived from a knowledge of the geology at the site (either the site at which the recordings were obtained or at which the estimate is required, or both). Figure 2 compares the estimated relationship between peak acceleration and distance from source obtained from a number of these proposed methodologies. In the zone where most of the data exist there is reasonable agreement. However, there is considerable variation in both the near source and far field. A few of the older methodologies give estimates notably lower than the rest.

Gutenberg and Richter's papers^{22,23} are important because they attempt to relate maximum acceleration to the energy released by earthquakes of different magnitudes. In Fig. 2 their estimates are much lower than the

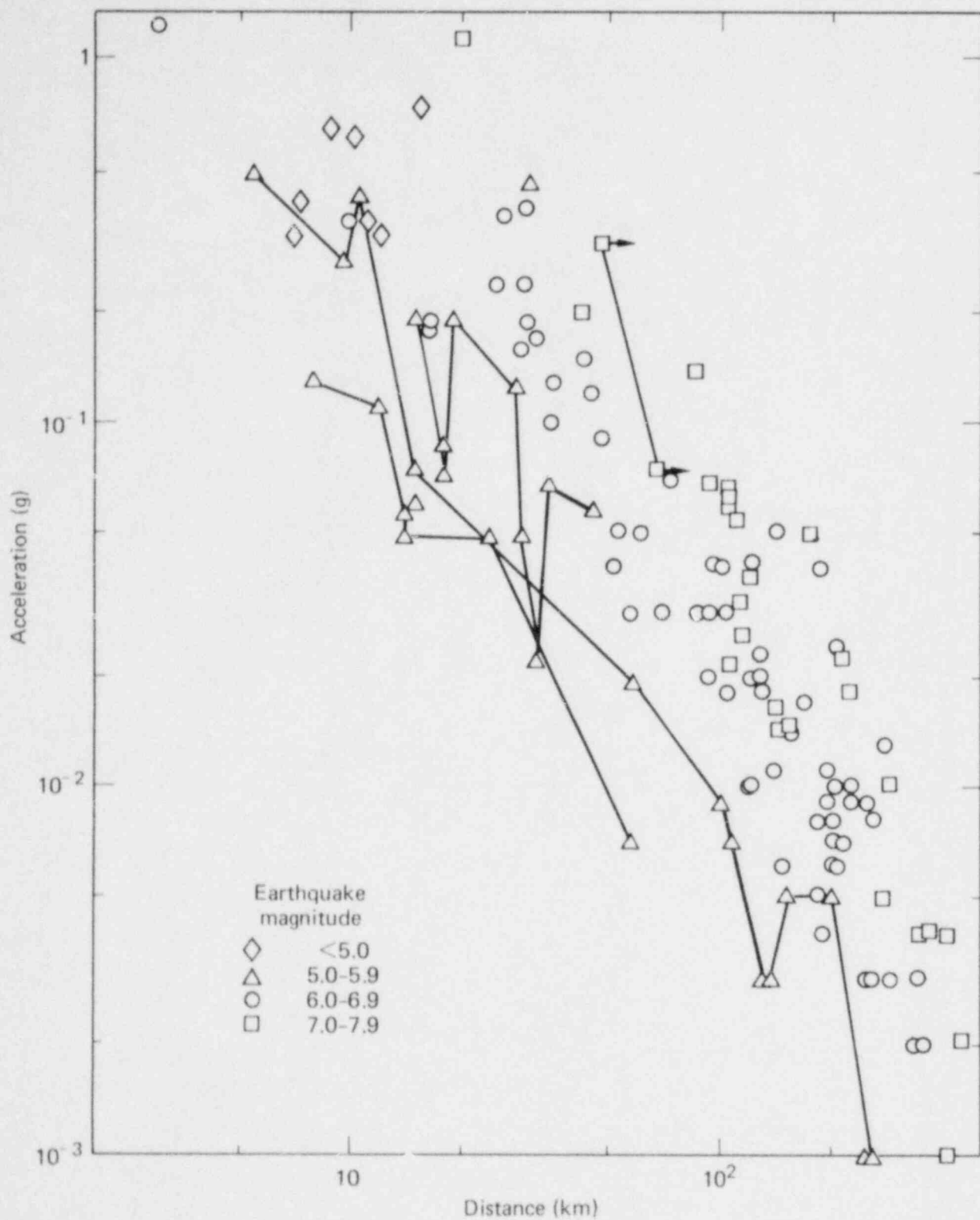


FIG. 1. Peak acceleration vs. distance for earthquakes of various magnitudes.

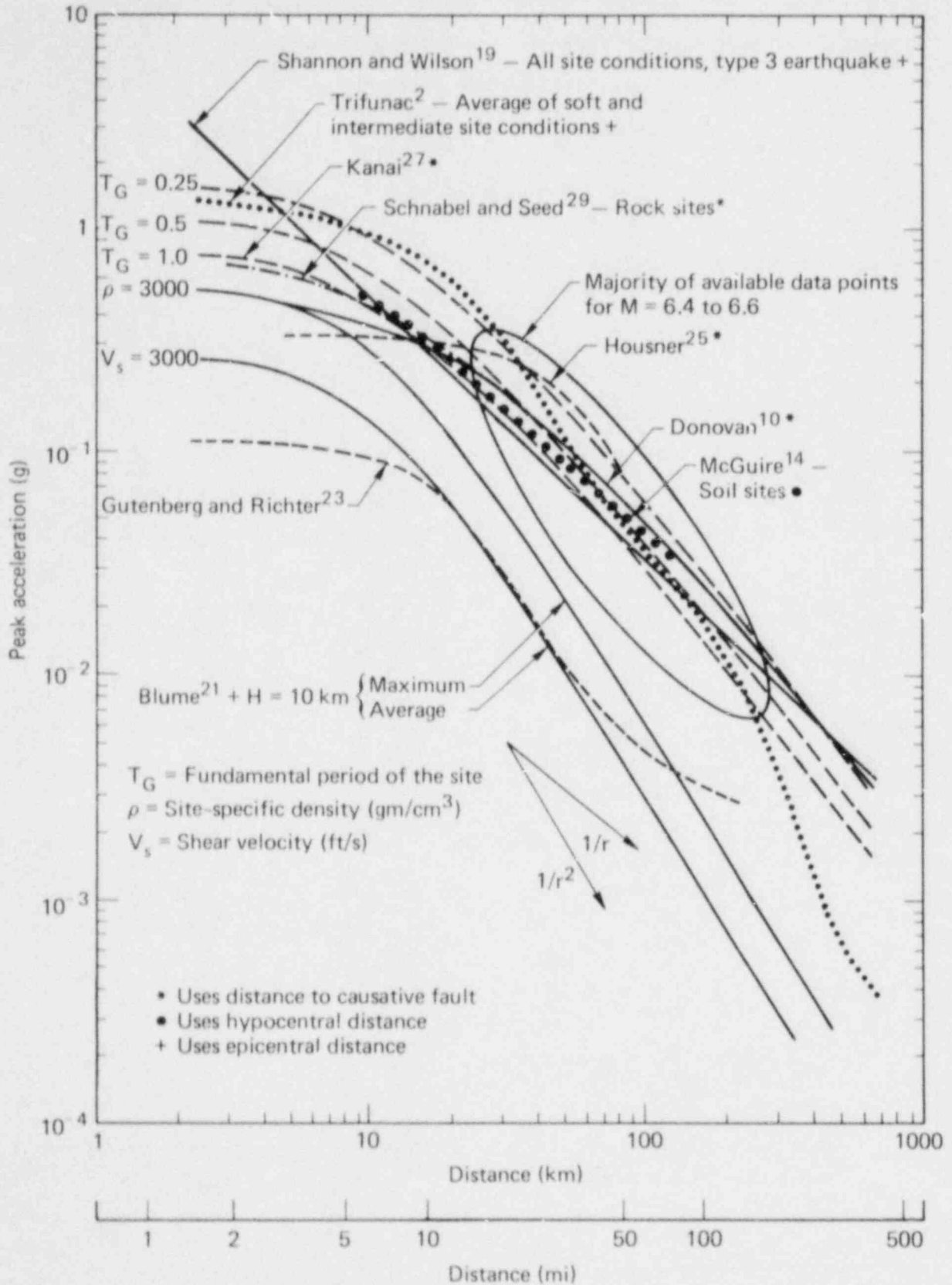


FIG. 2. Estimated relationship between peak acceleration and distance from source for magnitude-6.5 earthquakes.

actual data. One important reason is that they assumed that the peak acceleration is proportional to $(A_0/T_0)^2$, where A_0 is the estimated amplitude of the ground displacement near the fault and T_0 is the period. Gutenberg and Richter's approach also requires the assumption that earthquake magnitude and peak g value are directly related.

Housner²⁵ used the available data to attempt to develop empirical curves relating peak ground acceleration, distance, and earthquake magnitude. However, he had very few near-source data and very few data from large earthquakes. Housner's approach to bridge the important gaps in the data was to make an estimate of the near-source ground motion from a very large earthquake (the limiting case). He then used this estimate of the near-source acceleration to adjust the empirical curves developed at lower magnitudes and longer distances to obtain ground-motion estimates near the epicenters of both large and small earthquakes. To obtain this estimate, Housner arbitrarily assumed a pulse shape for the acceleration of the form

$$\begin{aligned}\ddot{u} &= A_1 \sin\left(\frac{\pi t}{t_1}\right) \quad 0 < t < t_1 \\ &= A_2 \sin\left(\frac{\pi t_1}{t_2}\right) \quad 0 < t_1 < t_0 ,\end{aligned}\tag{1}$$

where

$$t_1 = t - t_1 ,$$

$$t_2 = t_0 - t_1 .$$

Housner assumed that at time t_0 the velocity is zero and the displacement is equal to one-half the relative displacement (2D) across the fault. This gives

$$A_1 t_1 = \frac{\pi D}{t_0} ,$$

$$\dot{u}_{\max} = \frac{2A_1 t_1}{\pi} .\tag{2}$$

To obtain estimates of the maximum velocity, Housner assumed that near the fault the earthquake can be approximated by an instantaneous release of shear stress. This initiates a shear wave that propagates normal to the fault plane. A point on the ground nearby will experience a motion generated by the passage of a step-function shear wave (this assumption is much like the assumption made by Brune,³² discussed later). With this assumption Housner obtained the result

$$\dot{U}_{\max} = \gamma C, \quad (3)$$

where

γ = shear strain,

C = shear wave velocity.

It should be noted that this assumption gives infinite acceleration and does not agree with Housner's assumed pulse shape. Housner appeals to displacement data to obtain estimates of the shear strain.

As can be seen from Fig. 2, Housner's near-field estimates are low compared to recently recorded data. Other reasonable values of shear strain could be used in Housner's equations to get estimates in line with the recorded data. However, the basic form of his results gives little insight into the nature of the relation between the earthquake source parameters and the recorded ground motion, primarily because he assumed (1) that the peak acceleration scaled directly with magnitude, and (2) that a simple relation holds between peak acceleration, velocity, and final static displacement.

Hofmann²⁴ discusses a number of other studies that apply various modifications to the approaches taken by Gutenberg and Richter and by Housner. These give little additional insight into the relation between peak acceleration and earthquake magnitude.

Currently the United States Geological Service (USGS) typically refers to the work of Page et al.²⁶ to obtain estimates of near-field ground motion. The approach used by Page et al. was to look at the data from a number of earthquakes of various magnitudes and to infer the ground motion expected from future earthquakes of a similar magnitude. This approach gives little insight into the relationship between the parameters of interest; however Table 1, taken from their work, does give estimates of near-field ground motion.

TABLE 1. Near-fault horizontal ground acceleration.^a

Earthquake magnitude	Peak ground acceleration
8.5	1.25
8.0	1.20
7.5	1.15
7.0	1.05
6.5	0.9
5.5	0.45

^aPage et al.²⁶

Investigators such as Kanai,²⁷ Schnabel and Seed,²⁹ and Blume²¹ attempted to use site factors to account for the large variations observed between peak acceleration and earthquake magnitude. Data from a single earthquake such as the San Fernando event show that considerable scatter occurs because of such factors. Two interpretations can be given to such approaches. One is that corrections can be developed that can be applied to the "mean" curves developed by other investigators. Another interpretation is that by use of analyses such as those developed by Schnabel et al.³⁰ it would be possible to remove the local site effects and obtain "bedrock" estimates of the relations among magnitude, peak acceleration, and epicentral distance. The assumption is often made that such a correlation (if available) would greatly reduce the scatter of data.

Of the various approaches to site effects, the work of Seed and his co-workers is the most widely used. In particular the work of Schnabel and Seed²⁹ is cited in the NRC Standard Review Plan. They used records obtained from rock sites as well as a few computed rock motions from several earthquakes to obtain plots of acceleration, epicentral distance, and earthquake magnitude. Only the selected data from a few earthquakes were used. The shape of the curves through the data was obtained from a simplified analysis of the geometric attenuation and the effect of damping on attenuation. They assumed that the ratio of amplitudes of the various harmonics at distances R_1 and R_2 is a function only of the areas A_1 and

A_2 through which the energy flows and that the attenuation due to damping is of the usual form

$$a(r, f) = A e^{-\left(\frac{\pi f R}{QC}\right)}, \quad (4)$$

where

Q = Quality factor (assumed independent of frequency),

f = Frequency of harmonic of interest (Hz),

C = Appropriate wave velocity.

Schnabel and Seed combined these results to get the general shape of the attenuation of the ground motion. Using this shape and the data they chose as representative of earthquakes of various magnitudes, they constructed the estimates shown in Fig. 3. The upper and lower limits for each earthquake were obtained from the variation observed from the limited data they used to plot their curves. It is not clear how they obtained their estimate of the probable upper bound shown in Fig. 3.

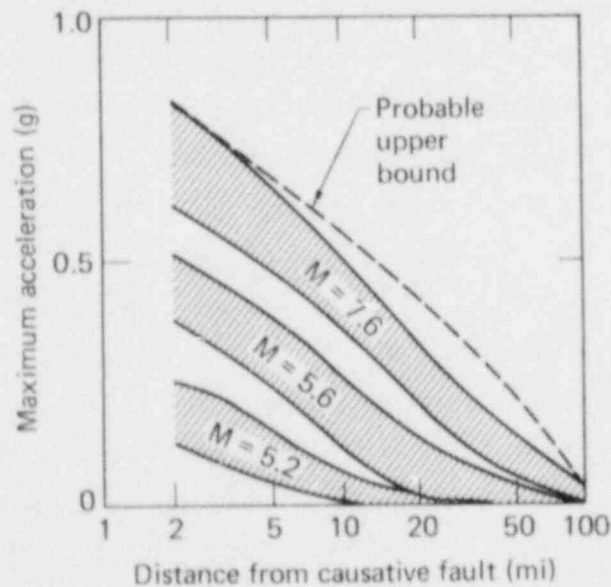


FIG. 3. Ranges of maximum acceleration in rock (Schnabel and Seed²⁹).

The difficulty with Schnabel and Seed's approach is that they assume that the magnitude of the earthquake is the most important parameter and that data from a few earthquakes are sufficient to fix the relationship (for rock sites) among peak acceleration, epicentral distance, and magnitude. Recent recordings of small earthquakes obtained in the near field greatly exceed Schnabel and Seed's estimates. Since several of these recordings are from rock sites, the difficulty cannot be attributed to amplification effects.

REGRESSION ANALYSIS APPROACHES

A number of studies fall into the Regression Analysis category (see Idriss for a complete review¹²). Typically, these studies assume that the ground motion scales directly with earthquake magnitude and distance. To obtain the required relation among earthquake magnitude, epicentral distance, and ground motion, some form for the functional relationship among the variables must be assumed. Considerable variation is introduced at this step. For example, McGuire^{14,15} has assumed

$$\log a = A + BM + C \log [f(R)] + DX_s, \quad (5)$$

where a is peak recorded acceleration (or velocity), A , B , C , D are constants, $f(R)$ is the assumed functional form of attenuation, and X_s is a site factor. This is a typical assumption. One of the major differences among the various correlations is the form assumed for attenuation with epicentral distance. For example, McGuire assumed that attenuation as a function of epicentral distance varies as $1/r^n$ and $1/(r + 25)^n$. Trifunac² assumed that the variation with r is the same as the one used by Richter in formulating his magnitude scale. Trifunac notes that this (and other) assumptions are arbitrary, and as such cannot be used to back-extrapolate the data into the near field. It should be noted that Trifunac² does not determine the attenuation from the regression analysis as is typically done (e.g., McGuire determines the value of the attenuation exponent n from the regression analysis).

One notable departure from Eq. (5) is the work reported in Ref. (19), where it is assumed that

$$\ln a \propto \frac{1}{M}$$

and such factors as site effects vary as

$$C_s \ln(r).$$

No explanation is given for these assumptions. However, as can be seen from Fig. 2, the results are similar to those of other studies. The assumption that $\ln a$ varies as $1/M$ reduces the influence of magnitude for larger-magnitude earthquakes. Sufficient data do not exist to determine whether this is an appropriate functional form.

Figure 4 compares correlations of Trifunac,² McGuire,¹⁴ and Donovan.¹⁰ The Trifunac and McGuire predictions are for rock sites, while Donovan's are for all types of sites. There are considerable differences among these correlations, particularly in both the near and far field, where

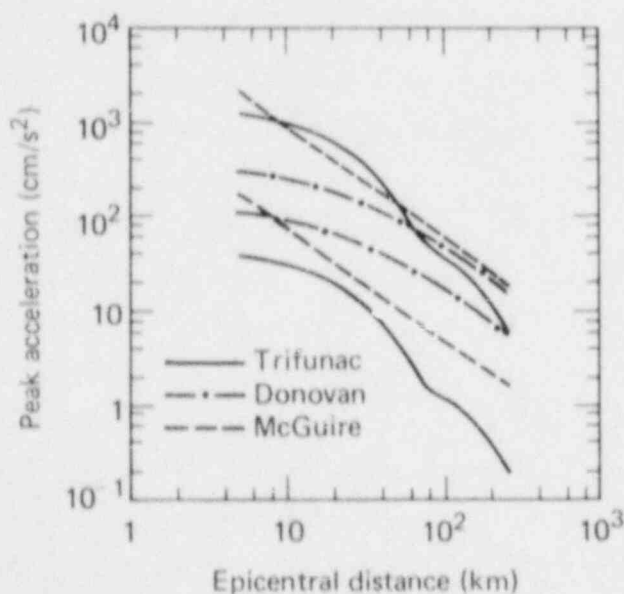


FIG. 4. Comparison of correlations between epicentral distance and peak acceleration obtained by Trifunac² to those of McGuire¹⁴ and Donovan¹⁸ for $M_L = 4.5$ and 6.5 .

fewer data exist. It should be noted that McGuire excluded near-field data. In Fig. 4 his work was extrapolated into the near field to make it simpler to distinguish the various curves.

There are a number of reasons for the differences among the different correlations. One major reason is the assumed form of attenuation. This is extremely important in both the near and far field. Another major difference is in the data set used. Donovan used world-wide data, Trifunac and McGuire used only U.S. data. In addition, McGuire only used a few of the San Fernando records and none of the near-field data. Also, considerable variation often exists in various data sets for the same earthquake. Generally the variation comes in the specification of the earthquake magnitude, the epicentral distance, and site type.

Table 2 gives typical equations obtained via regression analysis for earthquakes in various regions. Trifunac's results are not included because of the complex form he used; however, they are plotted in Fig. 4.

Ambraseys⁸ used 58 strong-motion records obtained at distances of 5 to 30 kilometers from European earthquakes of magnitude (M_L) 3.5 to 5 to develop a correlation of the form

$$\log a = 0.46 + 0.63 M - 1.1 \log R . \quad (6)$$

McGuire,¹⁴ using U.S. data, found the peak g value attenuated as $R^{-1.17}$; however, McGuire's data were primarily based on larger earthquakes at greater epicentral distances. They do suggest that the attenuation in Europe may be

TABLE 2. Typical results of regression analysis.

Reference	Data set	Equation	$\sigma_{\log a}$
McGuire ¹⁴	Western U.S.		
	Rock	$a = 30. \exp (0.89M)/R^{1.17}$	0.62
	Soil	$a = 25. \exp (0.89M)/R^{1.17}$	0.62
Donovan ¹⁰	Worldwide	$a = 1080 \exp (0.5M)/(R + 25)^{1.3}$	0.71
Ambraseys ⁸	European	$a = 2.88 \exp (1.45M)/R^{1.1}$	-
Esteva et al. ¹¹	Western U.S.	$a = 5600 \exp (0.8M)/(P + 40)^2$	0.64
Cornell et al. ⁹	Western U.S.	$a = 846 \exp (0.86M)/(R + 25)^{1.80}$	0.57

similar to that in the Western United States. Figure 5 compares Ambraseys's⁸ results to those of McGuire¹⁴ and Trifunac² for stiff site conditions at $M_L = 5$. As can be seen, Ambraseys's line lies well above Western U.S. data; however, because of the difficulty discussed earlier in comparing magnitudes of small earthquakes in two different geographical and geological regions, it is not possible to determine whether for an earthquake of the same "strength" the acceleration is in fact higher in Europe or whether the difference is simply a systematic bias in the scale used. For example, if $M_L = 5.5$ is used in either Trifunac's or McGuire's correlations there is little difference between European and Western U.S. data.

Somewhat more complex functional forms than Eq. (5) have been investigated by both McGuire¹⁴ and Trifunac.² However, they do not seem to improve the correlation. The models used by various investigators force a given magnitude dependence and attenuation dependence. As can be seen in Figs. 2 and 4, the assumed form of the attenuation used in the regression has a significant impact on both the near-source and far-field estimates of ground motion. Because the existing data set for both far field and near source is sparse and exhibits considerable dispersion, it is not possible to select the

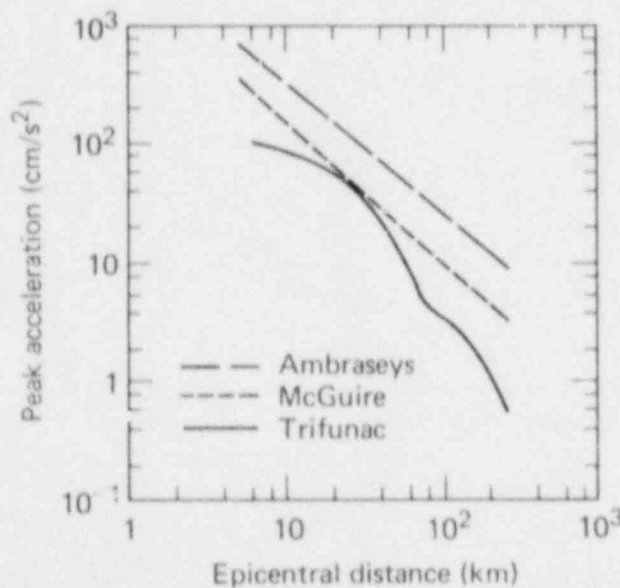


FIG. 5. Comparison of Ambraseys's⁸ correlation of epicentral distance and peak acceleration for Europe to those of Trifunac² and McGuire¹⁴ for $M_L = 5.0$ g.

correct functional form for attenuation from the available strong-motion data set. Thus it is important to know beforehand the correct functional form. (Later in this report we shall get an insight into the correct functional form by using explosion data.)

Typically, most regressions of the form of Eq. (5) show that

$$\ln a \sim 0.9 M$$

and

$$\sigma_{\ln a} \sim 0.7 .$$

Thus the ± 1 sigma zones almost overlap the mean estimates for earthquakes two magnitude units apart. This represents considerable dispersion, and makes it difficult to sort out the influence of magnitude on the ground motion, particularly in the near-source region, without resorting to modeling of some sort.

SIMPLE MODELING

Swanger et al.,³⁵ in their state-of-the-art review, subdivided the category we label Simple Modeling into two classes:

1. Kinematic Models - These models assume that the entire slip and rupture history of the fault is known. The slip history of the fault is all that is required to compute the seismic radiation. The details of the slip history, which are important to the high-frequency radiation, are sometimes included to satisfy some dynamic rupture constraint. Usually the details are dictated by a desire for mathematical simplicity.

2. Simple Dynamic Models - These models are analytic approximations describing some aspects of the stress-release process. They are normally used for interpretation of earthquake source parameters and for providing constraints on the characteristics of kinematic models. As these models are examined in detail by Swanger et al.,³⁵ our discussion here focuses only on a few key results.

One of the most useful approximations of a simple dynamic model was developed by Brune.³² To model near-field ground motion, Brune considered a tangential-stress pulse applied to an interior dislocation surface and assumed that during faulting a fractured surface does not transmit shear waves. He

further assumed that this pulse is instantaneously applied over a fault surface, and deliberately neglected fault-propagation effects. The stress pulse then sends a shear wave in a direction perpendicular to the fault surface. If x represents the perpendicular distance from the fault plane and $H(t)$ is the Heaviside unit-step function, the initial time and space dependence of this pulse is given by

$$\sigma(x,t) = \Delta\sigma H(t - x/\beta)$$

where $\Delta\sigma$ is the stress drop and β is the shear-wave velocity.

Ground displacement close to the center of the fault and in a direction parallel to the fault motion may be obtained by integrating the one-dimensional wave equation. Brune assumed that this model adequately approximates the first motions near the fault surface until the effects of the boundaries of the dislocation reach the point of observation. When this happens, particle velocity begins to decrease and gradually approaches zero. Brune approximately modeled this effect by introducing an exponential decay factor. Two important results from this simple model are: (1) the low-frequency behavior of the Fourier amplitude spectrum of the acceleration is controlled by the rupture length L , and (2) the peak spectrum amplitude is controlled by stress drop $\Delta\sigma$. The high-frequency behavior is not captured by Brune's model; however, Brune used his model to make estimates of the maximum acceleration in the near-field by considering the contribution of a finite band of frequencies from 0 to some cutoff frequency ω_s . Here Brune was using the observed fact that typically frequencies above 10 Hz do not significantly contribute to the peak acceleration observed. He obtained the result

$$a_{\max} = K \Delta\sigma \frac{\beta}{\mu} \omega_s,$$

where μ is the Lamé constant. Brune took $\omega_s = 10$ Hz and $\Delta\sigma = 100$ bars to get an estimate of 2 g.

The problem with Brune's estimate is that the high-frequency cutoff is very arbitrary. To overcome this difficulty, Trifunac² approximately modeled the high-frequency behavior of the Fourier amplitude spectrum of the ground acceleration. To avoid the arbitrary introduction of a new cutoff

frequency, Trifunac resorted to a complex argument based on the statistics of a series of oscillator responses to random excitation, arguing that the peak acceleration was proportional to the stress drop and to a factor accounting for duration (magnitude) effects. For typical earthquakes, Trifunac estimated that the peak g level would range from about 0.1 g (low-stress-drop earthquake) to about 5 g (high-stress-drop earthquake).

Hanks and Johnson⁴ simplified the basic equations of motion by assuming that the peak acceleration results from an isolated and localized faulting. In addition, they assumed that the peak acceleration decayed as L/r , where L is the radius of the localized region and r is the distance from the localized region. With these assumptions, they found

$$a = \frac{1}{\rho} \frac{\bar{\sigma}}{r},$$

where

a = peak acceleration,

r = distance from center of localized faulting,

ρ = density,

$\bar{\sigma}$ = dynamic shear-stress difference across localized faulting.

Hanks and Johnson⁴ used this result to explain the observation that in the near field the recorded peak g value is relatively independent of earthquake magnitude.

Other investigators^{8,20,36} have arrived at results similar to those of Refs. 2, 4, and 32, discussed above. These analyses explain the lack of correlation of the observed near-field peak g value with earthquake magnitudes; however, they are valid only very near the fault. The methodologies discussed earlier, which used magnitude as one of the independent variables, give estimates of the peak ground motion as a function of epicentral distance; however, for the reasons discussed, such correlations are not valid in the near field.

The studies by Kostrov,^{37,38} Madariaga,³⁹⁻⁴² Das,⁴³ Das and Aki,^{44,45} and Aki⁴⁶ developed simple rupture-propagation models that provide considerable insight. These studies suggest that stress and slip velocity concentrations exist in the vicinity of the fault's edges. These

stress concentrations radiate significant high-frequency energy when abrupt changes occur in slip velocity and/or stress levels.

Das and Aki⁴⁵ introduced a "barrier model" of earthquakes. Their studies show that the stress associated with P and S waves traveling ahead of the crack tip can cause fault slip in the case of an inplane shear (but not tensile) crack with a finite cohesive force. They show that the same mechanism plays a key role in generating a complex rupture process when obstacles, barriers, or asperities exist on the fault plane, offering a unified theory for a variety of seismic source functions.

Das and Aki characterize a barrier by measures of its areal extent and of the magnitude of its strength. If the areal extent is large, the crack tip propagation will be stopped. But if the areal extent is small in comparison to the instantaneous crack size at the time of encounter, the crack tip and the barrier will interact in the following three different ways, depending on the magnitude of barrier strength relative to tectonic stress:

1. If the tectonic stress is relatively high, the barrier is broken as the crack tip passes.
2. If the tectonic stress is relatively low, the crack tip proceeds beyond the barrier, leaving behind an unbroken barrier.
3. If the tectonic stress is intermediate, the barrier is not broken at the initial passage of the crack tip but eventually breaks because of subsequent increase in dynamic stress.

Thus the presence of barriers on the fault plane will introduce diverse slip functions and a variety of seismic wave forms. Das and Aki's numerical experiments⁴⁵ illustrate some important consequences of the barrier model. First, it offers a physical basis for the idea of "multiple shocks" (Wyss and Brune,⁴⁷ Trifunac and Brune⁴⁸). Second, it explains why the stress drop should increase with magnitude, as evidenced in the scaling laws for seismic spectra of small earthquakes in several areas (Aki and Chouet⁴⁹). Third, it explains why the simple uniform dislocation model in which a common slip function is propagated often gives results in good agreement with observations. If the fault has many equally spaced barriers and the rupture front propagates by neither breaking barriers nor stumbling on them, the seismic motion will be indistinguishable from that of the uniform dislocation model.

Some care must be taken when comparing values of stress drop determined by different approaches. This is discussed in some detail by Madariaga.⁴¹ The static stress drop is generally defined by the relation

$$\Delta\sigma = \frac{M_0}{CSW}, \quad (7)$$

where

M_0 = seismic moment,

S = fault area,

W = fault width.

The seismic moment is generally obtained from the long-period limit of the Fourier spectrum of the displacement time series of the body waves in the far field. Typically it is determined using the approximation

$$\Delta\sigma = \frac{M_0}{CL^3} \quad (8)$$

where the equivalent fault radius L is determined by use of Brune's model and the Fourier spectrum of the recorded displacement. The parameter L is determined from the observed corner frequency. The corner frequency is the frequency of transition of the seismic displacement spectrum from the flat shape at low frequencies to the asymptotic decay at high frequencies. The location of the corner frequency is a function of some characteristic dimension of the source. This relationship is crucial in stress drop estimation, since for a given seismic moment the inferred stress drop is inversely proportional to the third power of the characteristic dimension. In other words, an error of a factor of two in the characteristic dimension causes a difference of a factor of eight in inferred effective stress. There has been great debate within the seismological community over what observed corner frequencies are and how they are related to the characteristic dimensions of the source.^{39,41,50}

Madariaga³⁹ compared the corner frequencies assumed by Brune with those produced by propagating circular shear cracks. Brune assumed an azimuth-independent relationship between corner frequency and fault radius. Madariaga showed that this average value may be in error at certain angles off

the fault plane by 50 percent for the instantaneous forming shear crack, and possibly by as much as 100 percent for subsonic ruptures.

Brune et al.⁵⁰ suggest that the differences in corner frequencies noted by Madariaga may be due only to differences in the way corner frequencies are determined from spectral data. Since most of our measurements of effective stress come from corner-frequency measurements, there is still much uncertainty as to what values of stress drop are appropriate for earthquakes. This confusion is heightened if one considers estimates of the stress drop made from near-source records, which often yield stress drops much higher than those obtained by use of far-field data. One simplified explanation for this is as follows. Before the moving stress-wave concentration associated with the fault tip reaches a point X_0 along the fault, the local stress is equal to the tectonic stress σ_T . When the local dynamic stress concentration reaches the ultimate strength of the fault gouge, σ_u , the fault ruptures locally and the stress drops rapidly to σ_F , the dynamic frictional stress on the fault. The static stress drop is given by

$$\sigma_T - \sigma_F.$$

However, the high-frequency radiated energy is locally controlled by the "dynamic" stress drop

$$\sigma_u - \sigma_F.$$

The ground motion recorded near the source is likely to be governed by the dynamic stress drop and the location of barriers or other factors that would change the rupture velocity or stress drop. As the distance from the source increases, the local variations along the fault "average out."

CALCULATIONAL APPROACHES

The studies of Madariaga and Das fall somewhere between the simple modeling category and the calculational category. Other more complex finite-element and finite-difference approaches are reviewed in Ref. 35 and will not be discussed here, as they provide little additional insight into the relation of earthquake source parameters and observed ground motion.

SCALING RULES

None of the above results is very satisfactory. They do show that the stress drop is an important parameter, but the actual relation between the calculated stress drop and the recorded peak g value is not specifically given. What is needed is a methodology that combines the earthquake source parameters with appropriate attenuation laws to provide useful predictions of strong motion.

The approach taken here is to derive scaling rules enabling comparison of the observed ground motion from earthquakes having different source parameters. Appropriate attenuation equations of the strong ground motion are then developed from available data. The attenuation relations are combined with the scaling rules to obtain a general equation that gives the peak ground motion as a function of the earthquake source parameters and the hypocentral distance. The resulting methodology is verified by comparing predicted results to recorded ground motion for a number of earthquakes.

Scaling rules⁵¹ have been developed for explosions, and several investigators^{5,36} have used somewhat similar approaches for earthquakes. For example, Dieterich³⁶ used a finite-element model and scaling laws to study the relation of the observed ground motion to the earthquake source parameters. In his analysis of the scaling laws, Dieterich assumed that the characteristic length was related to the mesh size required to calculate a given frequency. He developed the relation

$$\ddot{U} = k \Delta\sigma \omega \frac{\beta}{\mu}$$

where

k = constant,

ω = cutoff frequency in the calculational mesh,

β = shear velocity,

μ = Lamé constant.

Dieterich then normalized peak acceleration with stress drop to show that this reduced the scatter in the data.

Our approach is similar; however, characteristic lengths and times are interpreted in a different way. To obtain the desired relations, we consider

for simplicity only one region (see Fig. 6), which will have a larger dynamic stress drop and/or change in rupture velocity than the surrounding fault zone. This assumption is similar to the one made by Hanks and Johnson. In terms of the Das-Aki barrier model, the zones of interest are the barriers where rupture velocity goes locally to zero and rapid changes in stress drop occur. A large earthquake might be characterized by several such zones. For the near-source ground motion, the zone of most significance would be the zone closest to the point of observation of the ground motion. Clearly, in actual practice several zones might overlap, and the observed ground motion would best be explained by some average equivalent zone. The May 18, 1940 Imperial

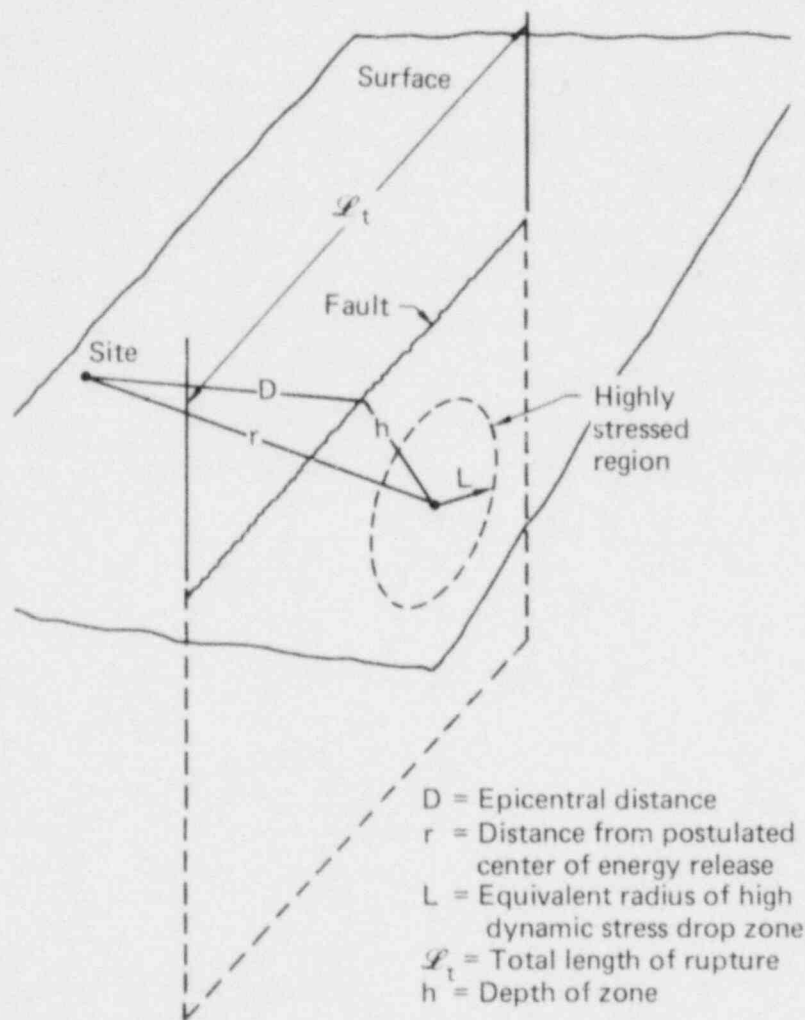


FIG. 6. Simplified model of fault zone with region of high dynamic stress, used to develop scaling rules.

Valley earthquake is a good example of such complex behavior.⁴⁸ For seeking scaling parameters we assume that:

1. All the various mechanisms which contribute to the radiation of higher-frequency seismic energy can be represented by a single parameter, which we will call "stress drop."

2. The regions of high stress drop are suitably separated. In "Discussion of Results" we examine the physical nature of the parameter $\Delta\sigma$. To obtain scaling relations we further assume that the velocities and displacements are sufficiently small so that the equations of motion can be written in the linear form

$$\rho \frac{\partial^2 U_i}{\partial t^2} = \frac{\partial \sigma_{ij}}{\partial X_j} + \bar{X}_i, \quad (9)$$

where

U_i = displacement of the i th coordinate,

σ_{ij} = stress.

The particle velocity v_i is given by

$$v_i = \frac{\partial U_i}{\partial t}$$

and the particle acceleration is given by

$$a_i = \frac{\partial^2 U_i}{\partial t^2}.$$

In these equations the usual summation convention relative to the indices is used.

We know little about the mechanics of the actual faulting process; hence we hope that the rupture process is sufficiently similar between events so that the exact details are not important. This is the same general assumption made by Brune³² and by Aki^{46,52} in developing their simplified source models. Even the more complex calculational approaches implicitly make this assumption.

We seek the appropriate scaling parameters for Eq. (9) to render the solutions similar; this also requires us to assume that the rupture process is similar for different problems. To obtain the scaling rules, we introduce the transformations

$$U_i^* = \frac{U_i}{a}, \quad t^* = \frac{t}{c}, \quad \sigma_{ij}^* = \frac{\sigma_{ij}}{b}, \quad \rho^* = \frac{\rho}{\rho_0}, \quad \text{and}$$

$$X_i^* = \frac{X_i}{d} \tag{10}$$

into Eq. (9), which becomes

$$\frac{\partial^2 U_i^*}{\partial t^{*2}} = \frac{bc^2}{\rho_0 da} \frac{1}{\rho} \frac{\partial \sigma_{ij}^*}{X_i^*}.$$

For dynamic similarity, we need

$$\frac{bc^2}{\rho_0 ad} = \text{constant}.$$

For simplicity, it's reasonable to assume that $b = \Delta\sigma$ and $d = L$. Here $\Delta\sigma$ refers to the maximum dynamic stress drop and L is the equivalent radius of the most highly stressed region. The time parameter enters the problem through the dynamics of the boundary condition of the highly stressed area. Since we assume that this process is similar between events, the characteristic time should scale as $c = L/\beta_r$, where β_r is the rupture velocity. We assume that β_r is proportional to the shear velocity β and in the following equations use β in place of β_r . Making these substitutions in the above equations, we find that

$$a = \frac{\Delta\sigma L}{\rho_0 \beta^2}.$$

If the values for the scaling parameters (a, b, c, d) are used in Eq. (10), we get

$$U_i^* = U_i \frac{\rho_o \beta^2}{\Delta \sigma L} , \quad (11)$$

$$v_i^* = \frac{v_i \rho_o \beta}{\Delta \sigma} , \quad (12)$$

$$\alpha_i^* = \frac{\alpha_i L \rho_o}{\Delta \sigma} . \quad (13)$$

These are the rules for scaling between events; that is, for relating the ground motion parameters among various earthquakes. These results are similar to Dieterich's,^{5c} except that he interpreted the characteristic length L as the mesh size in his calculation and scaled time as a function of frequency.

It is important to note that we did not invoke a linear relation between stress and strain; such a relation provides no additional scaling parameters.

In the above analysis, a number of important factors were not directly considered. For example, the geometry of the problem can be important, since we know that in the far field there is a complex radiation pattern that is governed by the fault geometry parameters and the location of the site (both distance and azimuth) relative to the faulting process. It is not known how important this is in the near field. No doubt it will, in part, contribute to the scatter of the data. The differences in travel path and the local site conditions are known to be extremely important. The depth of the energy release can have considerable influence on the material properties as well as on the body-force term X_i in Eq. (9). The body force was neglected, but large differences in the depth of the earthquake may be significant. The dip of the fault may be an important parameter; however, it is possible that the variation is small enough so that the effect is small compared to the other effects.

The list of restrictions is so imposing that one might conclude that the approach is of limited value. On the other hand, it may be that many of the factors we listed as important are really only second-order effects and that the ground motion is primarily a function of a few main variables. Clearly it is possible to answer these questions only by empirical means.

Considerable data from underground explosions (UGE)--both nuclear and conventional--verify the basic utility of scaling. This is illustrated in Fig. 7 relative to the peak acceleration for a number of explosions using scaling rules similar to Eqs. (11)-(13). These data and similar studies (many unpublished)⁵³⁻⁵⁵ show that:

1. The scaling rules are valid; i.e., one can scale between very small and very large events, even in the highly nonlinear regime.
2. Material properties are important. This is particularly true in the strong-motion regime.

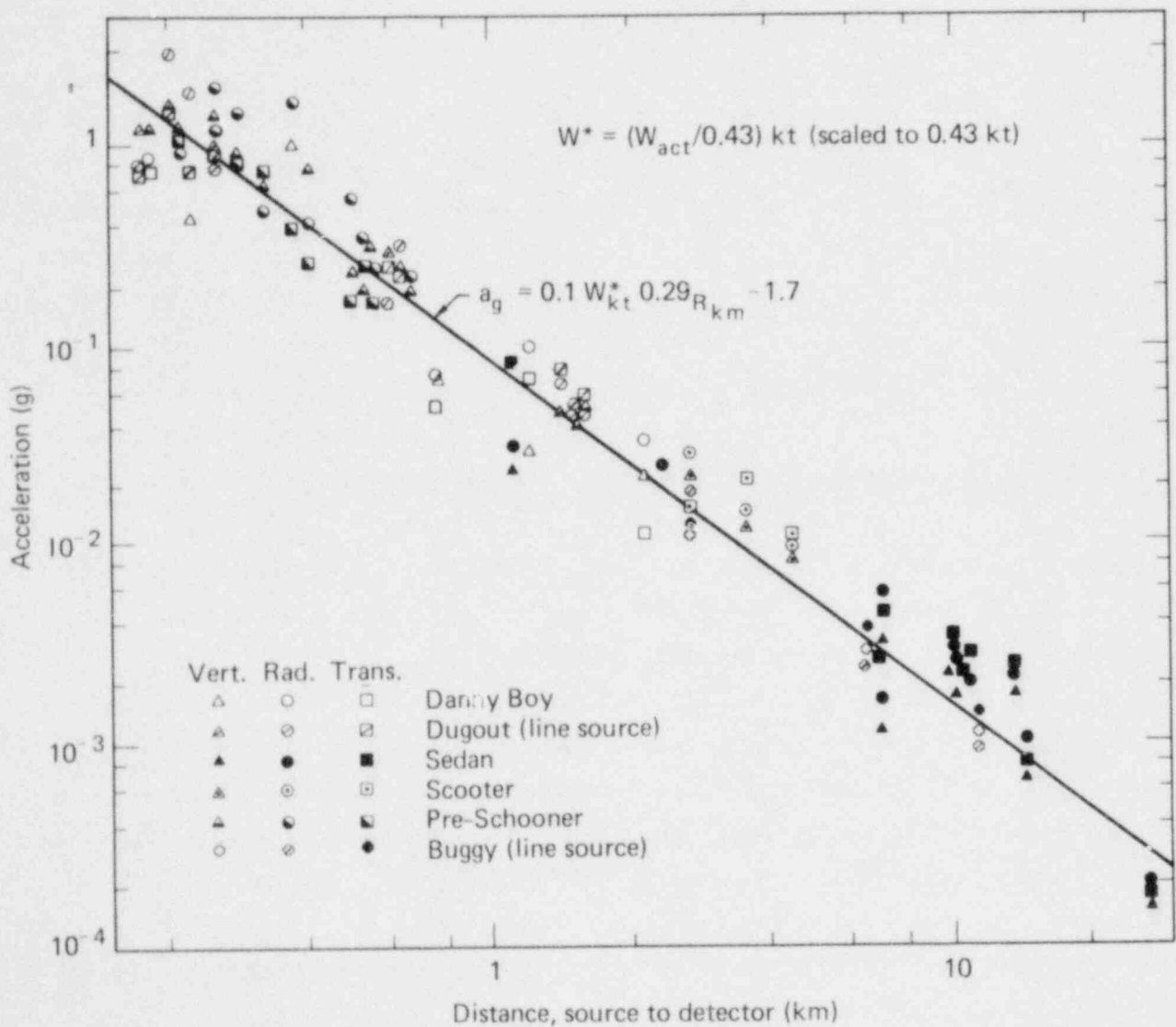


FIG. 7. Comparison of scaled peak acceleration from a number of explosions of different sizes.

3. Travel path/site effects do introduce considerable scatter; however, the scatter is not so great as to negate the usefulness of the correlations.

4. Body forces are important for large differences in overburden.

The data from UGE are useful in that they verify the basic concept of scaling. The major question left unanswered is: Do different earthquakes display a similar dynamic faulting process? That is, among the various basic types of fault movement--strike-slip, thrust, normal, etc.--is all faulting of a given type similar with respect to the dynamic process involved? Further, it is also possible that the type of faulting processes is a second-order effect relative to the basic scaling parameters, thus enabling us to scale among all types of earthquakes. (It should be noted, for example, that Brune's source model, which has been so fruitful for various types of earthquakes, implicitly contains the assumption that differences in the faulting process are second-order effects.)

ATTENUATION

In order to be able to make comparisons between ground motion from various earthquakes, we need a methodology to extrapolate--for a given earthquake--the observed ground motion into the near field. The problem is too complex to directly derive the appropriate law; however, for UGE considerable data exist to show that

$$a(r) = \frac{A_0}{r^n}, \quad (14)$$

where A_0 is a function of the medium, yield, etc., and r is the range from the explosive source.⁵³⁻⁵⁵ Figures 8 and 9 show typical results.^{56,57}

Only for a few earthquakes are there sufficient data that could be used to verify Eq. (14), many in the far field. It is not clear that Eq. (14) is valid in the near field, since unlike explosions, which are point sources, earthquakes are line sources. In the far field this difference is not important, but clearly could be in the near field. Because so few earthquake data exist in the near field, it is not possible to directly assess these potential difficulties. However, some data exist for salvo-type

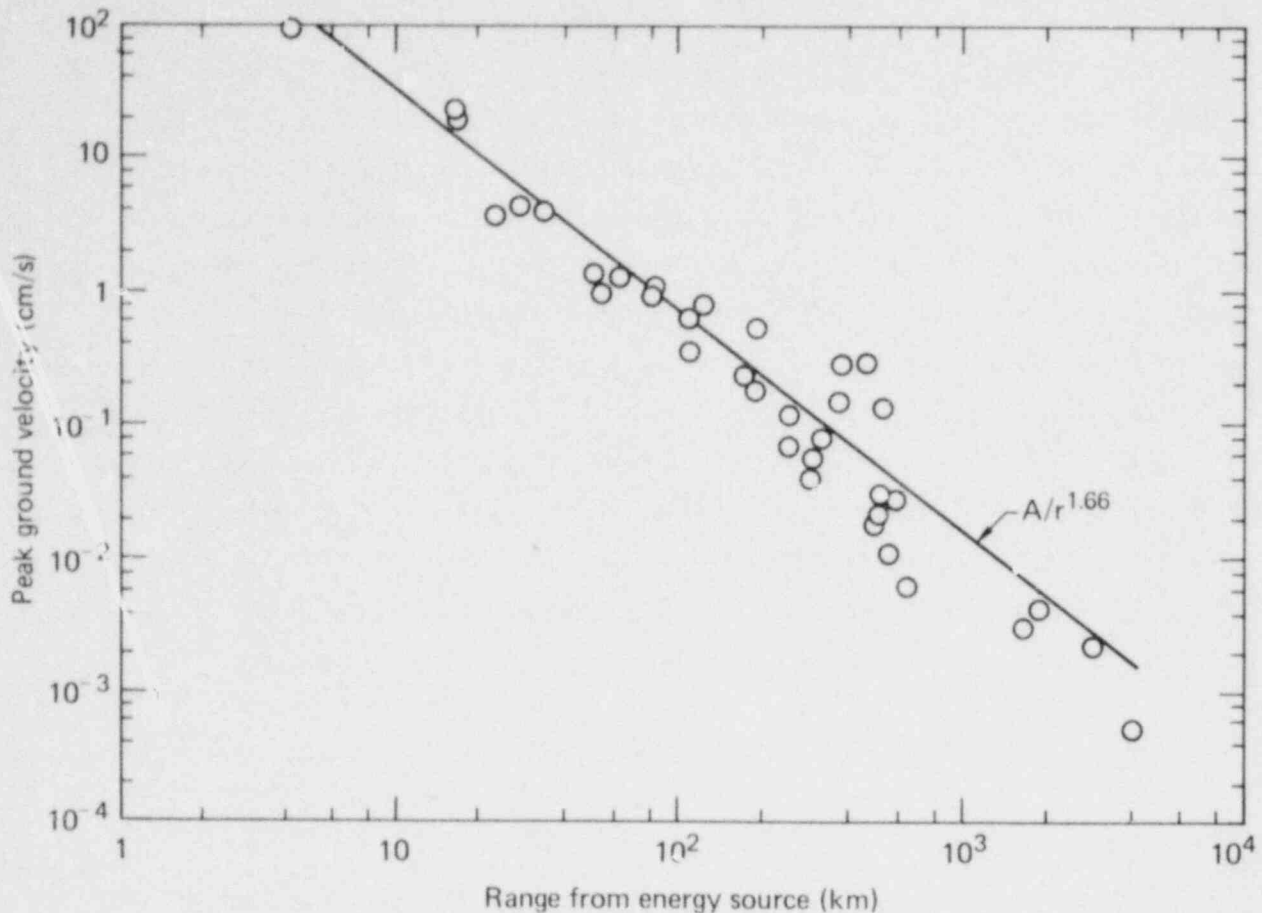


FIG. 8. Attenuation of peak ground velocity, "Boxcar" explosion.

explosions used to study the feasibility of creating a canal via explosives. Table 3 lists the most useful of these.

Figures 10 through 14 show the recorded peak velocity as a function of range. It is seen that the velocity attenuates as $1/r^n$. Peak surface acceleration was not typically measured over sufficient distances to make the same comparisons from the far field to the very near field. Figure 14 is of considerable interest, as for this array the density of the charge in each hole was sufficiently small so that very near-field measurements were obtained. That is, for the other array the nearest measurement was at a distance $r/L \sim 0.25$, where L is the length of the array and r the distance from the center of the array. It is seen that the law A/r^n is valid for distances of r/L as small as 0.25. For smaller distances, significant departure from this attenuation law is observed.

We conclude from these data that it is reasonable to back-extrapolate data into the near field using the relation A/r^n . This extrapolation may be

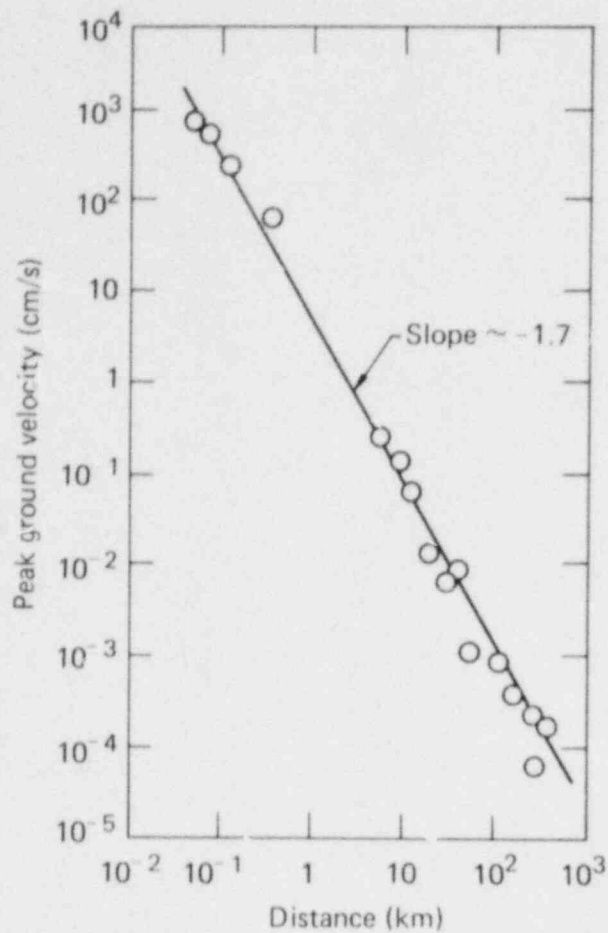


FIG. 9. Attenuation of peak ground velocity, "Danny Boy" explosion (0.43 kt, single device).

TABLE 3. Earthquake-related data, salvo explosions.

Event	No. of charges	Spacing (m)	Yield of each charge (kt)	Length line source (m)	Ref. No.
Dugout	5	13.7	0.02	55 (180')	58,59
Buggy	5	46.0	1.1	180 (590')	60,61
Pre-Gondola II	5	6.6	0.02	100 (320')	62,63
Dip IIA	29	2.2	0.0014	61 (200')	64
Dip VA	16	22.0	0.0025	346 (1136')	65

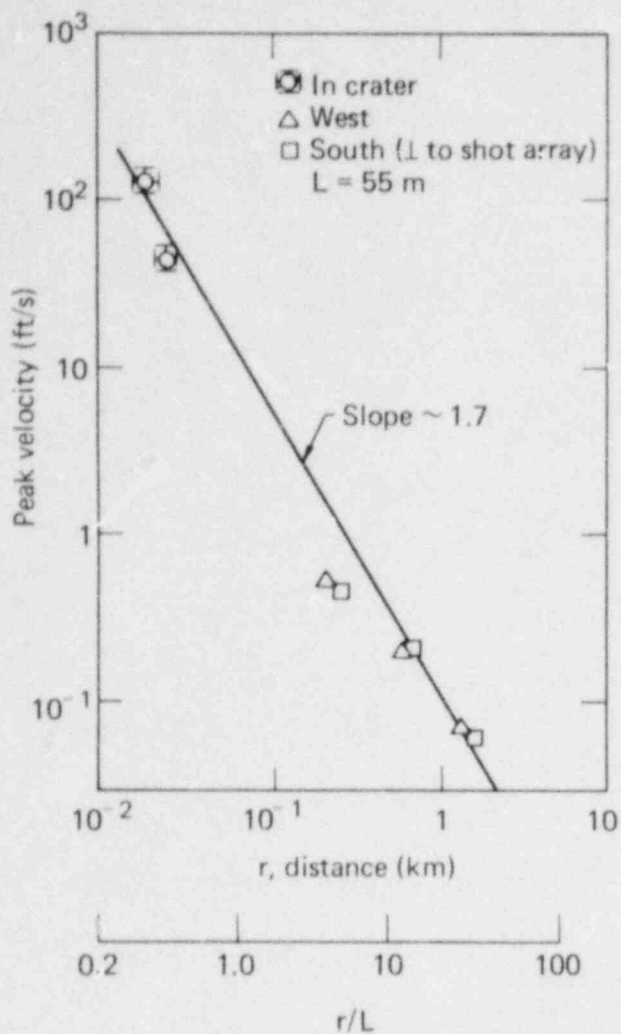


FIG. 10. Attenuation of peak ground velocity, "Dugout" explosion--salvo of five 0.02-kt devices, line source of 0.55 km (180 ft).

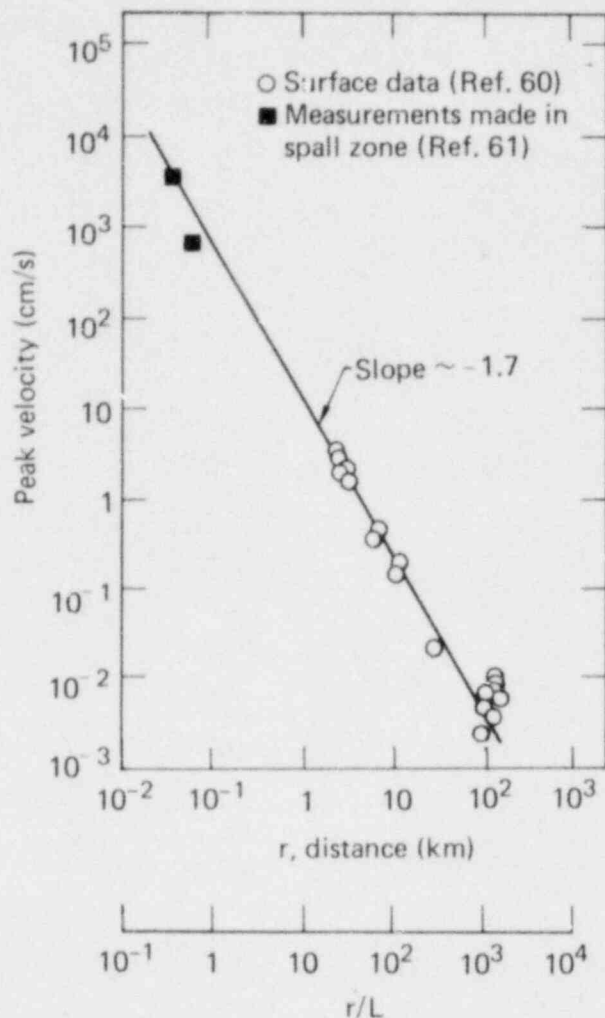


FIG. 11. Attenuation of peak ground velocity, "Buggy" explosion--salvo of five 1.1-kt devices, line source of 0.18 km (590 ft).

valid for distances as close as $r/L \sim 0.25$. The above results do not prove that the rule suggested by Eq. (14) is valid for an earthquake; however, they do suggest that it is a reasonable choice.

BASIC EQUATIONS AND VERIFICATION

Using Eq. (14) and assuming it is possible to scale between earthquakes, we can write

$$a^*(r^*) = \frac{A^*}{(r^*)^n}, \quad (15)$$

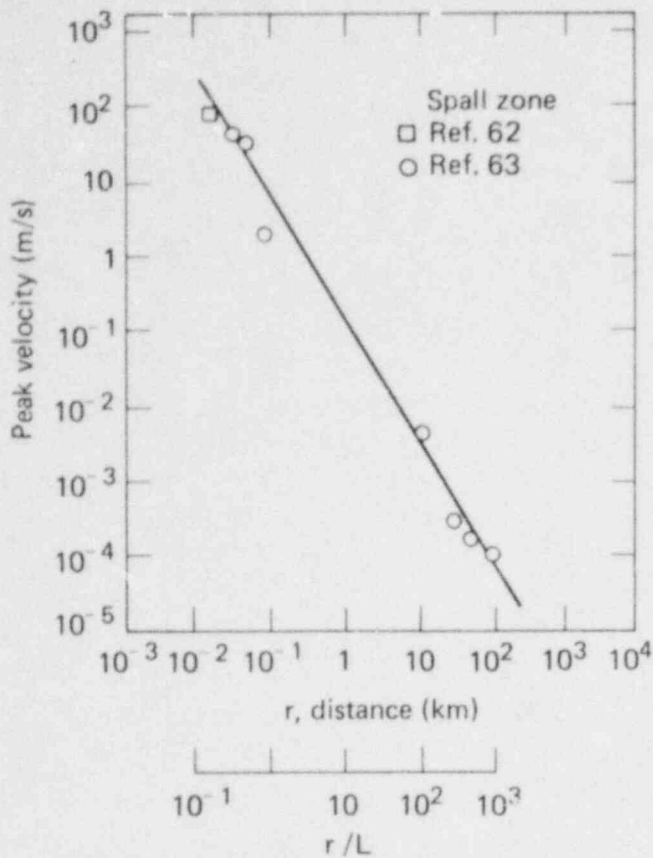


FIG. 12. Attenuation of peak ground velocity, "Pre-Gondola II" explosion--salvo of five charges, $L = 0.1$ km (320 ft).

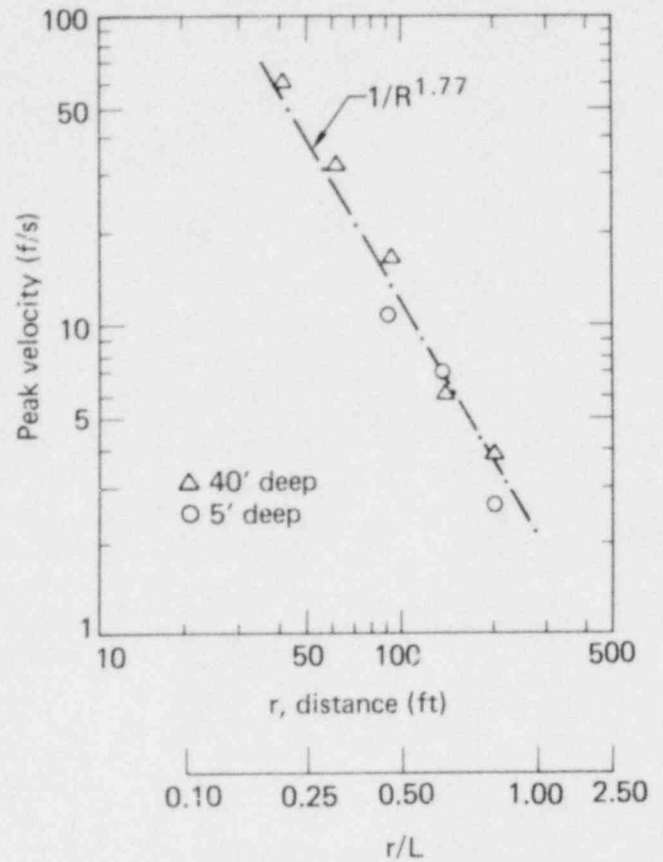


FIG. 13. Attenuation of peak ground velocity, "Dip IIA" explosion-- $L = 0.07$ km (200 ft); 0.04 kt.

where A^* is a function only of the medium and the depth of energy release. Hence, introducing Eq. (13) and $r^* = r/L$,

$$a_{\text{recorded}} = \frac{A^* \Delta \sigma L^{n-1}}{\rho_o r^n}; \quad (16)$$

thus

$$\log \frac{aL\rho_o}{\Delta \sigma} = \log A^* - n \log \frac{r}{L}. \quad (17)$$

Two sets of data can be used to determine whether there is dynamic similarity in the faulting process. The first comprises the main event and

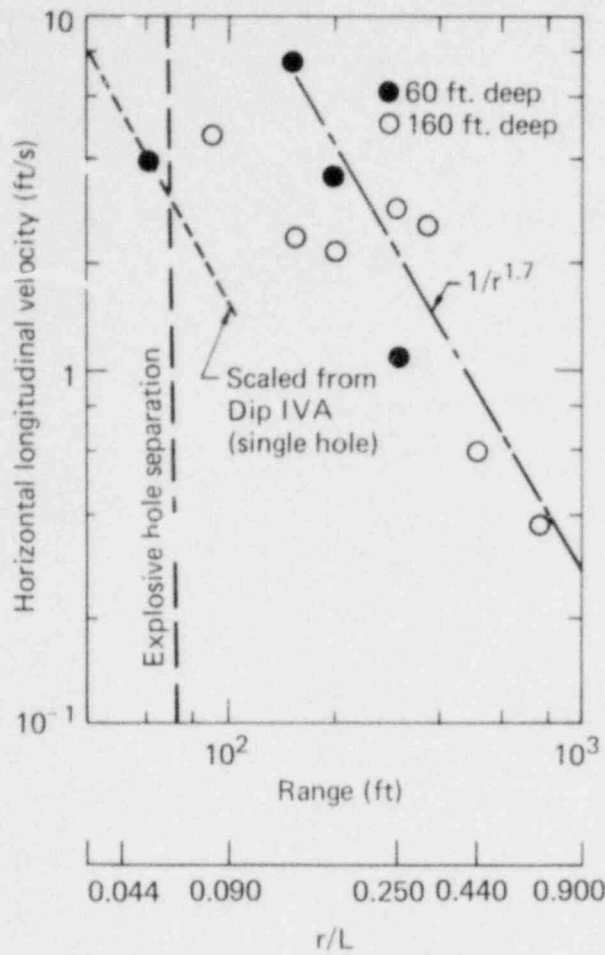


FIG. 14. Longitudinal centerline peak velocities, "Dip VA" explosion-- $L = 0.38$ km (1136 ft) $\cdot 0.04$ kt.

initial aftershocks of the 1971 San Fernando earthquake.⁶⁶ All of these events were recorded at the Pacoima Dam site, and thus provide a number of earthquakes with similar travel paths. The second set comprises the main shock and aftershocks of the 1940 Imperial Valley earthquake recorded at El Centro.⁶⁷ The San Fernando earthquake was on a thrust fault, whereas the Imperial Valley earthquake was on a strike-slip fault. These data will thus allow us to assess the importance of the faulting type.

Trifunac^{66,67} examined the main shock and aftershock sequence at these two sites and determined the dynamic stress drop and the fault dimension L of the highly stressed region hypocentral distance r , using Brune's source model and the Fourier spectra calculated from the recorded acceleration time histories. Trifunac also determined the magnitudes of the various aftershocks

from the strong-motion accelerograph data. These data are given in Tables 4 and 5. Figures 15 and 16 show the fit of Eq. (17) to the two sets of data for $\rho_0 = 1$. Table 6 gives the coefficients n and A^* for the two sets of data. Several important results can be noted:

1. The fit of Eq. (17) to the data is excellent, considering the uncertainty associated with the calculation of each of the parameters.
2. The attenuation coefficient is for practical purposes the same for both sets of data.

The constant A^* is larger by a factor of two at the El Centro site. It is useful to determine whether this difference can be related to the basic earthquake mechanism (thrust faulting for the Pacoima Dam site and strike-slip for the El Centro site) or is due to site/material properties. We can correct for material properties in Eq. (17) by introducing ρ_0 . We can then determine whether dynamic similarity exists by use of Eq. (17); i.e., by scaling both sets of data as suggested by Eq. (16). If there is similarity in

TABLE 4. Source parameters calculated by Trifunac⁶⁶ for the San Fernando earthquake and initial aftershock.

Event	$\Delta\sigma$	Peak accel.	r	L	M_L
Main	100	1.25	7	10	6.6
1	502	0.12	18	0.88	5.5
3	30	0.02	12	0.56	4.3
4	227	0.06	15	0.36	4.9
5	72	0.04	13	0.42	4.6
6	29	0.02	11	0.56	4.4
9	111	0.04	9	0.22	4.4
10	98	0.09	12	0.74	4.8
11	307	0.11	12	0.45	5.4
16	29	0.04	7	0.73	4.4
17	23	0.01	11	0.56	4.3
22	69	0.03	12	0.63	4.6
30	48	0.03	17	0.69	4.6
31	20	0.02	14	0.93	4.3

TABLE 5. Source parameters calculated for the El Centro earthquake and initial aftershock.⁶⁷

Event	$\Delta\sigma$	Peak accel.	R	L	M_L
1A	177	0.36	14	2.3	5.9-6.1
1B	186	0.28	15	1.5	6.-6.1
1C	143	0.23	16	1.8	5.8
2	349	0.15	35	3.2	6.5
3	63	0.02	24	1.2	4.8-5.1
4	16	0.015	18	1.3	4.4
5	12	0.02	12	1.1	4.4
6	103	0.02	39	1.2	5.4
7	23	0.01	30	2.2	4.6-5.0
9	57	0.08	16	1.7	5.1-5.2
10	30	0.016	17	0.8	4.6-4.7
11	217	0.07	33	1.2	5.8-5.9

TABLE 6. Coefficients A^* and n in Eq. (17) obtained by a least-squares fit to data in Tables 4 and 5.

Data	$\text{Log } A^*$	n	Fig. No.
San Fernando (S.F.)	-1.18	-1.75	15
El Centro (E.C.)	-0.89	-1.809	16
Combined:			
$\rho_o = 1$ (S.F.)	-1.1	-1.77	17
$\rho_o = 0.67\rho_{pd}$ (E.C.)			

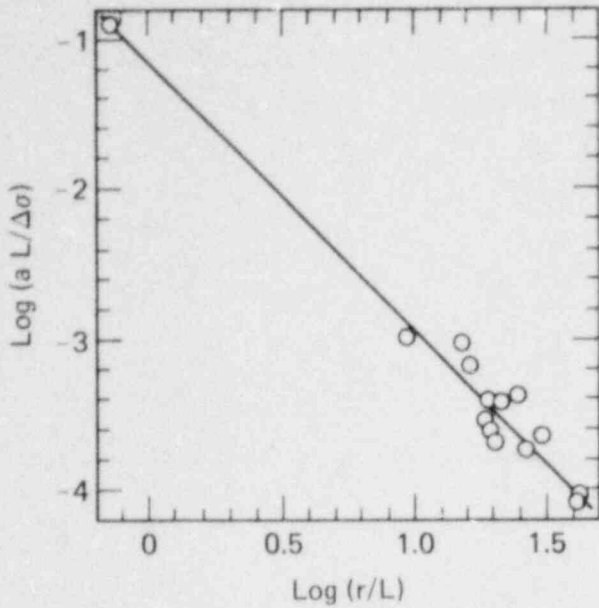


FIG. 15. Fit of San Fernando earthquake data (Table 4) to Eq. (17) using parameters in Table 6.

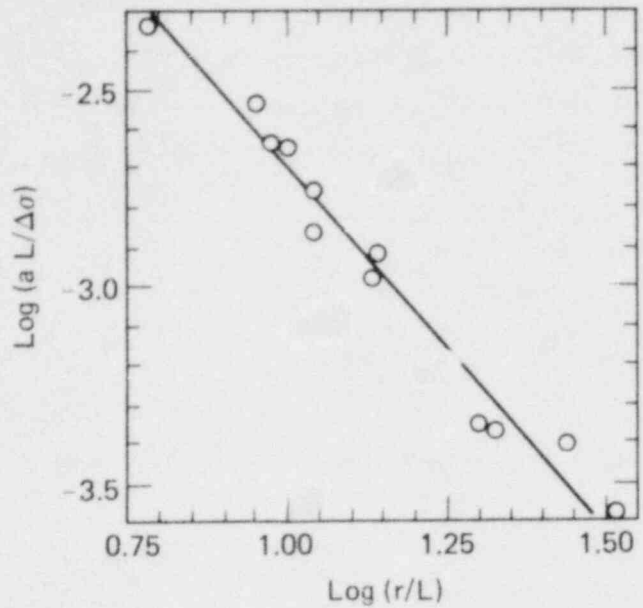


FIG. 16. Fit of May 1940 El Centro earthquake data (Table 5) to Eq. (17) using parameters in Table 6.

the dynamic faulting process--or at least if the differences among thrust, strike slip, and whatever mechanism is involved in the aftershock sequences have only a second-order effect on the main ground motion parameters--then there is a single universal value for A^* and for n in Eq. (17). For simplicity, we take $\rho_o = 1$ for the Pacoima Dam (PD) data and scale the data at El Centro (EC) by

$$\rho_o \equiv \frac{(\mu/\beta^2)_{EC}}{(\mu/\beta^2)_{PD}} . \quad (18)$$

Trifunac⁶⁷ did not give the values of (μ/β^2) he used to calculate the stress drop for the El Centro site. However, the appropriate value can be back-calculated from the data and figures given in his paper. Our calculations suggest that the appropriate value of the ratio (18) to use for our scaling is

$$\rho_{EL} \approx 0.67 \rho_{PD} . \quad (19)$$

As our fits to the data were "eyeballed," with large error bars, our value for Eq. (18) may be different from Trifunac's. However, we feel that our fits are as "good" as those he used. Figure 17 shows the combined data set (Pacoima Dam and El Centro), scaled as discussed. The fit of Eq. (17) to the data shown in Fig. 17 is

$$\log \frac{a \rho_0 L}{\Delta \sigma} = -1.1 - 1.77 [\log (r/L)] . \quad (20)$$

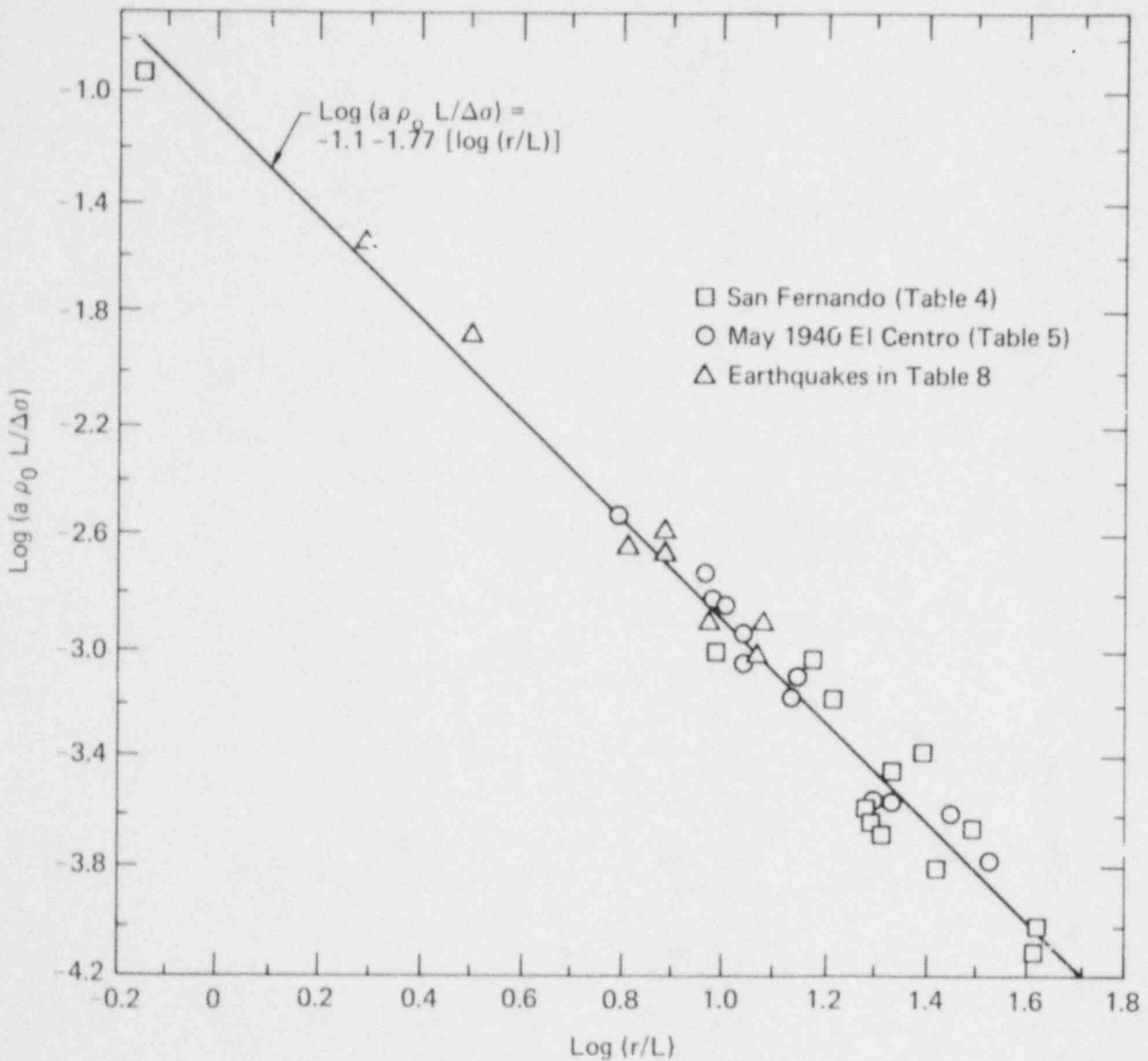


FIG. 17. Combined fit of San Fernando and El Centro earthquake data to Eq. (17); scaled using $\rho_0 = 1.0$ (rock), $\rho_0 = 0.67$ (soil), and parameters in Table 6.

We see that the fit is excellent, considering how poorly many of the parameters are known.

Equation (20) can be written as

$$a = \frac{0.071 L^{0.77} \Delta\sigma}{\rho_0 r^{1.77}} \quad (21)$$

Equation (21) can now be compared to the recorded data from several earthquakes, listed in Table 7. To use Eq. (21), it is necessary to have consistent values for the stress drop and the length of faulting involved. These values can be obtained in a manner similar to the approach used by Trifunac.^{66,67} For each of the earthquakes listed in Table 7, the Fourier amplitude spectrum is given in Ref. 68 at a number of stations. We typically chose one or two stations per earthquake, usually the station nearest the

TABLE 7. Earthquakes used to verify Eqs. (21) and (25) and the source parameters obtained via a fit of Brune's model to selected Fourier spectra obtained from strong-motion accelerograph data.

Earthquake	M_L^a	$\Delta\sigma$	L
Lytle Creek	5.7	240	1.6
Borrego Mt.	6.9	450	6.0
Kern County	7.2	300	6.0
San Francisco	5.3	90	1.6
Parkfield	5.9	120	4.0
San Fernando	6.4	600	3.0
Imperial Valley	(6.4) ^b	100	6.9
Coyote Lake	(5.7) ^b	160	1.3

^a Values determined by Kanamuri and Jennings.⁸³

^b Initial value for M_L based on far-field data.

epicenter. The appropriate fault length and stress drop were obtained from the best fit of Brune's³² source model

$$\log \left(\frac{\text{Fourier amplitude}}{\text{spectrum}} \right) = \log \left(2 \Delta\sigma \frac{\beta}{v} \frac{L}{r} R\theta\phi \frac{\omega^2}{\omega^2 + \alpha^2} \right), \quad (22)$$

where

$$\alpha = 2.34 \beta/L,$$

$$R\theta\phi = \frac{2}{\pi} \text{ (the value used by Trifunac),}$$

to the Fourier amplitude spectrum of the recorded acceleration. The factor of 2 accounts for the free surface effect.

We first made an initial estimate of L from the spectrum. Then, knowing the acceleration, we obtained an initial estimate for the stress drop from Eq. (20). Often, several iterations on both $\Delta\sigma$ and L were required to get an adequate fit. No particular criterion was used to determine whether the fit was acceptable, as it was felt that the scatter in data and local site effects are so large that it would be pointless to use a complex least-squares fitting process. The final values of $\log(a\beta_0 L/\Delta\sigma)$ for each earthquake, also shown in Fig. 17, fall on the line given by Eq. (20).

The source parameters $\Delta\sigma$ and L obtained for a particular earthquake were then used in Eq. (21), which gives the peak acceleration for the earthquake as a function of r. These predicted values were then compared to the actual recorded values.

Figures 18, 19, and 20 show the fit of Eq. (22), using the parameters given in Table 7, to the Fourier spectra computed from the recorded ground motion at selected stations for the earthquakes listed in Table 7.

Trifunac^{66,67} applied a correction of the form

$$\exp \frac{\pi fr}{Q\beta},$$

with $Q = 150$ and $\beta = 3.5$ km/s, to spectra computed from the strong-motion records. When $r > 20$ km we also applied this correction at selected frequencies. These corrected points are shown in Figs. 18 and 19 by the solid

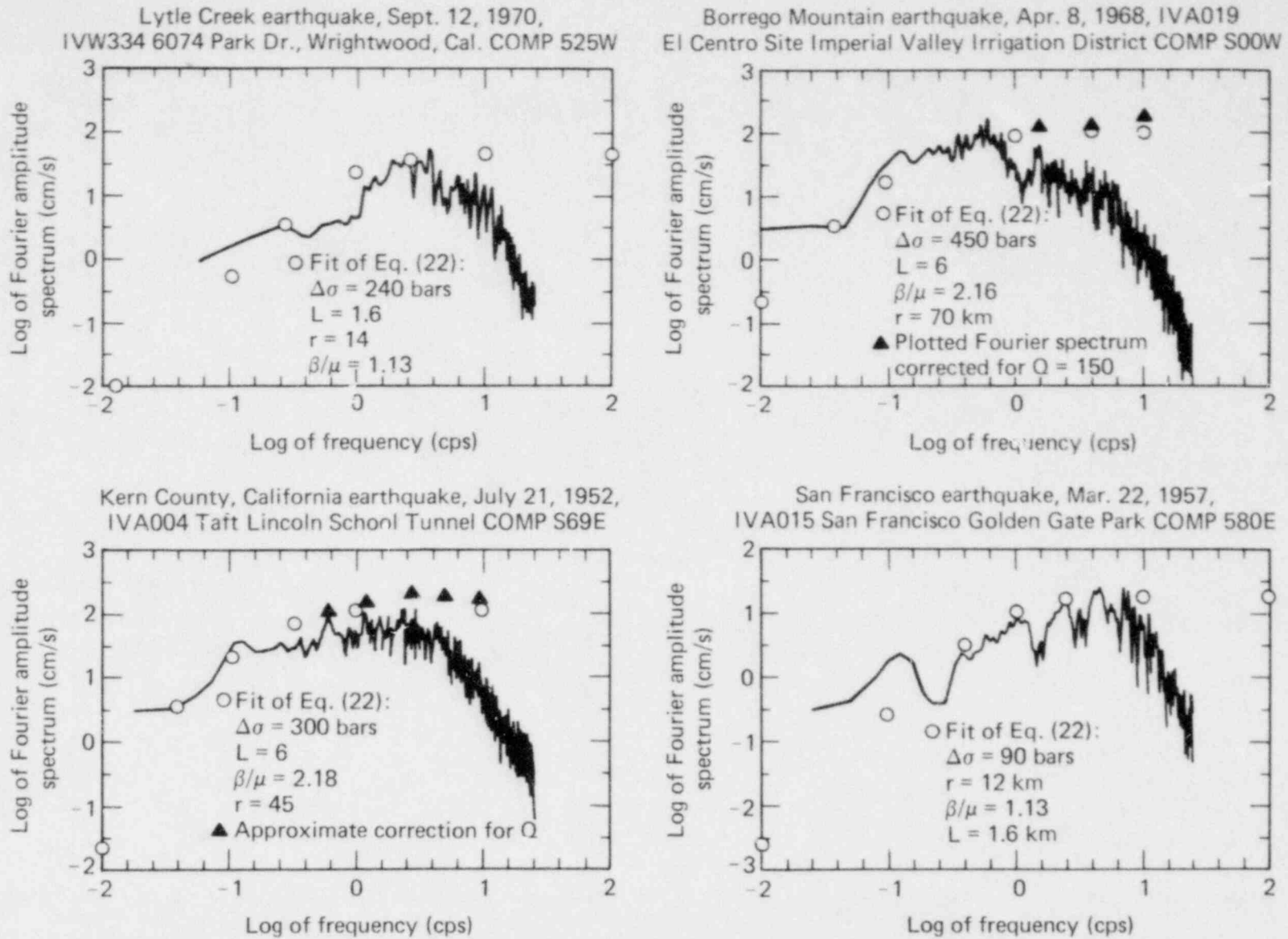
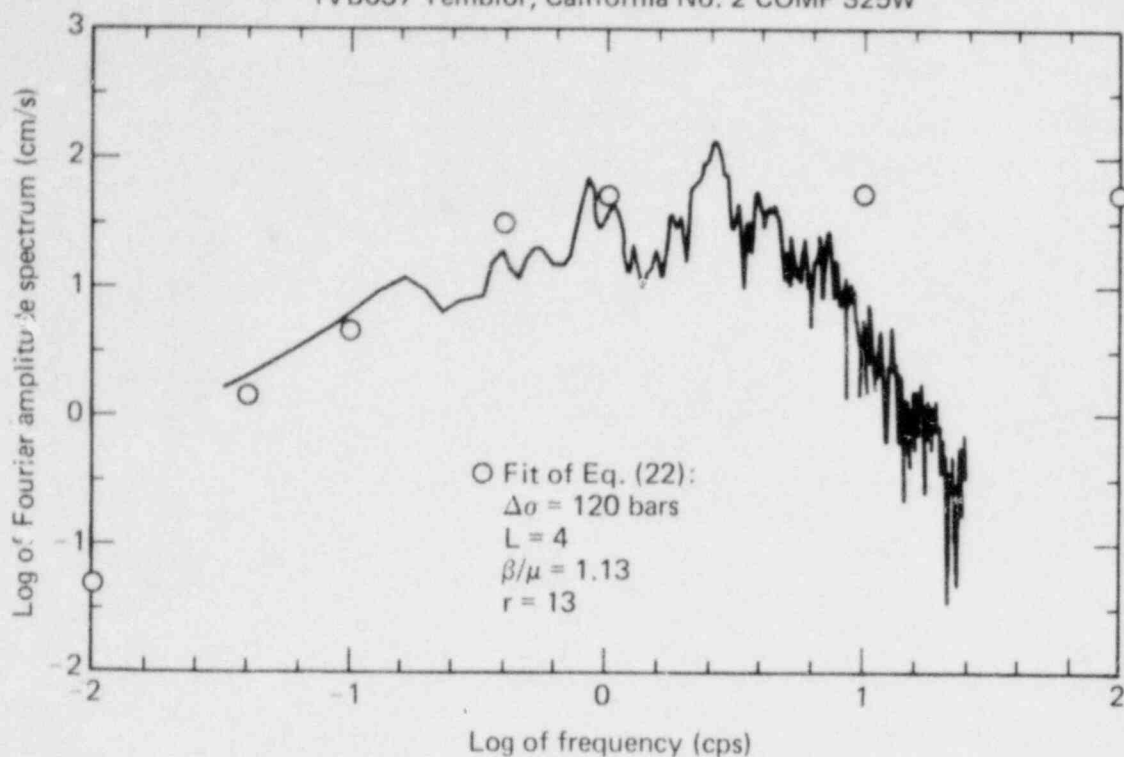


FIG. 18. Fit of Eq. (22) to Fourier amplitude spectra of acceleration, various earthquakes.

Parkfield, California earthquake, June 27, 1966, 2064 PST.
 IVB037 Temblor, California No. 2 COMP S25W



San Fernando earthquake, Feb. 9, 1971, 0600 PST.
 IV0198 Griffith Park Observatory, Moon Room, Los Angeles, Cal. COMP S00W

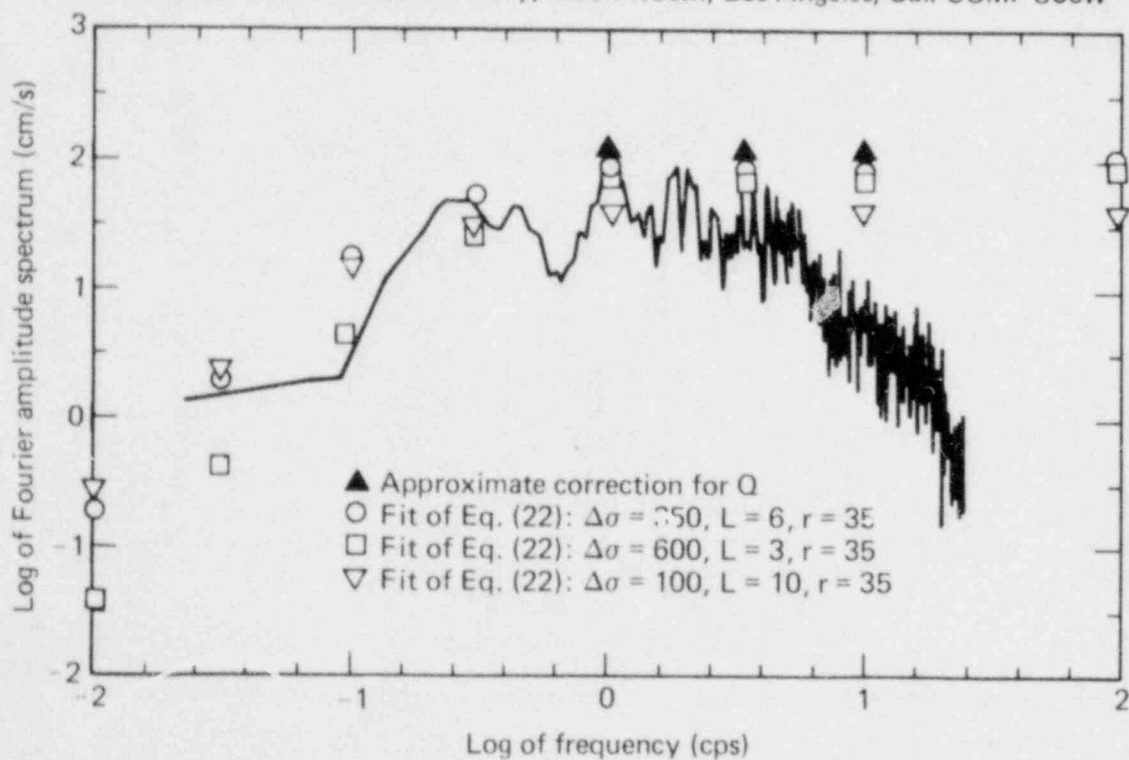


FIG. 19. Fit of Eq. (22) to Fourier amplitude spectra of acceleration, Parkfield and San Fernando earthquakes.

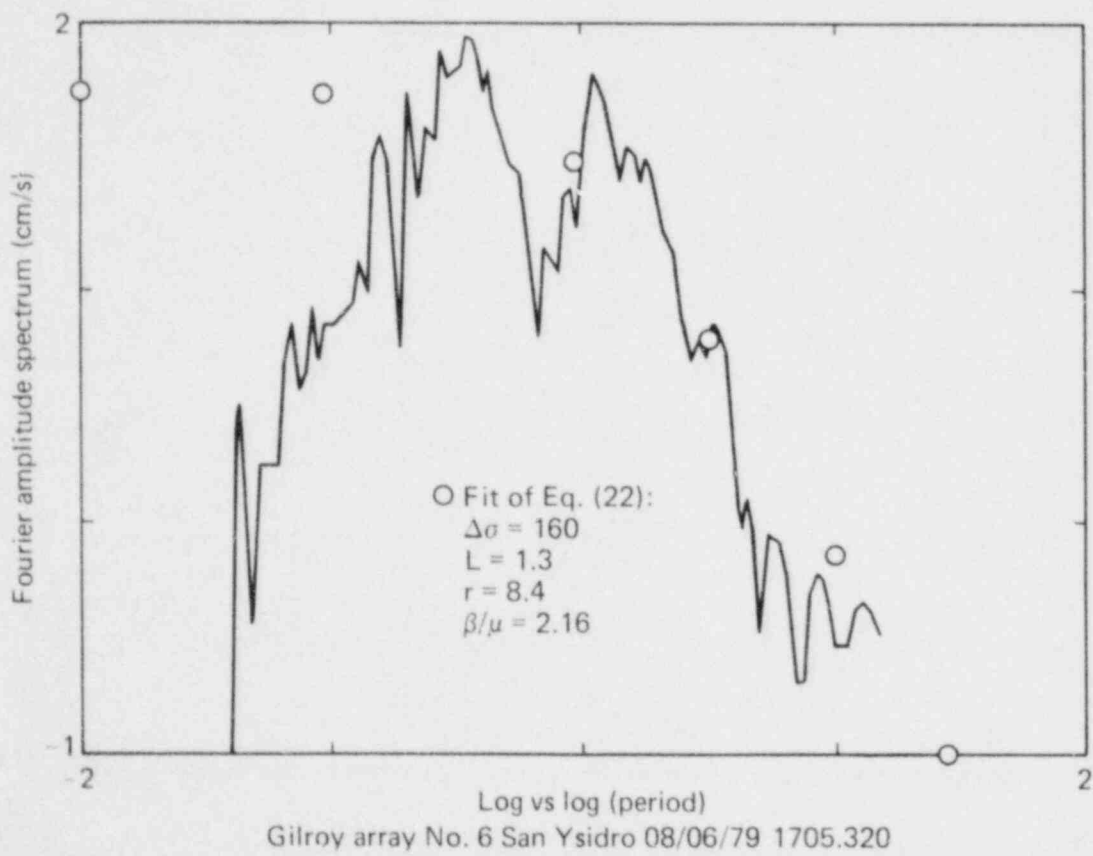
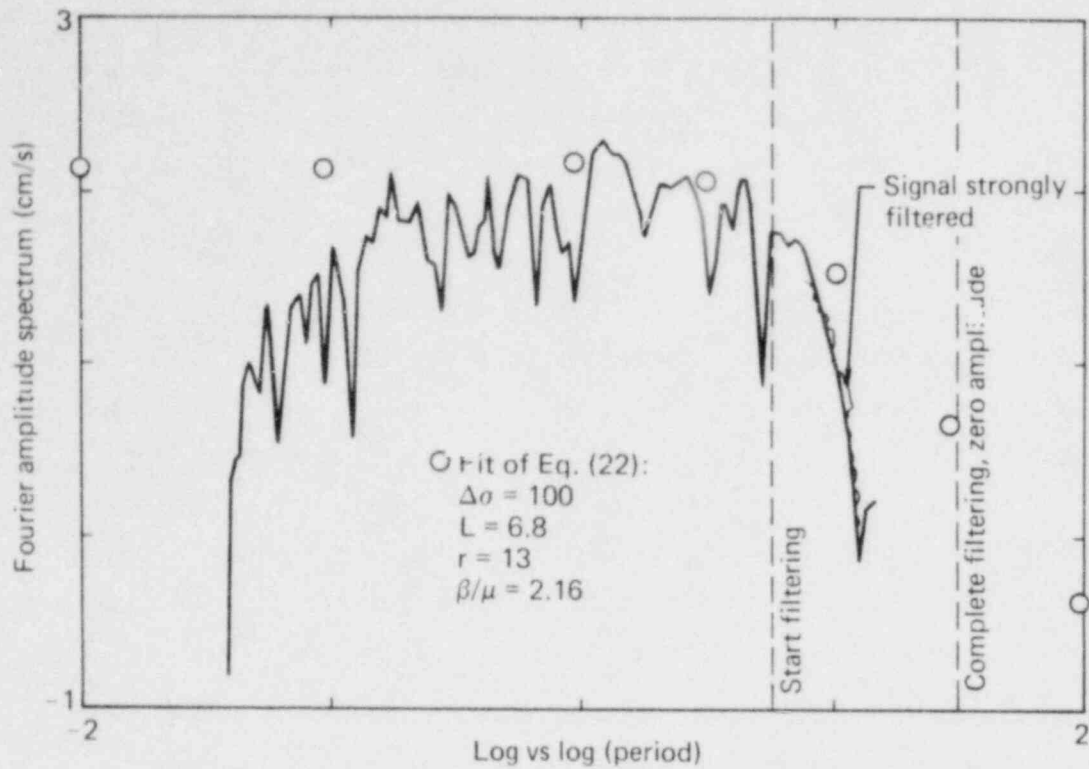


FIG. 20. Fit of Eq. (22) to Fourier amplitude spectra of acceleration, Imperial Valley and Gilroy earthquakes.

triangles. For $r < 20$ km the correction is unimportant for the earthquakes considered and hence is not shown in Figs. 18, 19, and 20.

Figures 21-28 show the comparison of Eq. (21) using the parameters given in Table 7 to the actual recorded accelerations. The fit is good, considering the limitations of the analysis and the wide range of earthquake magnitude and distances included.

There are several possible choices for the distance of the El Centro site from the Borrego Mountain earthquake of April 9, 1968. Our analysis of the strong-ground-motion data results in an estimate of $L = 6$ km, in reasonable agreement with the results of Burdick and Mellman⁶⁹ and Heaton and HelMBERGER.⁷⁰ The results of Refs. 69 and 70 suggest that the localized region of high stress drop was near the epicenter. For this reason we have placed the center of energy release for the Borrego Mountain earthquake at the epicenter, which puts the El Centro station approximately 60-70 km away. It should be noted that surface rupture did extend about 20-30 km closer to the

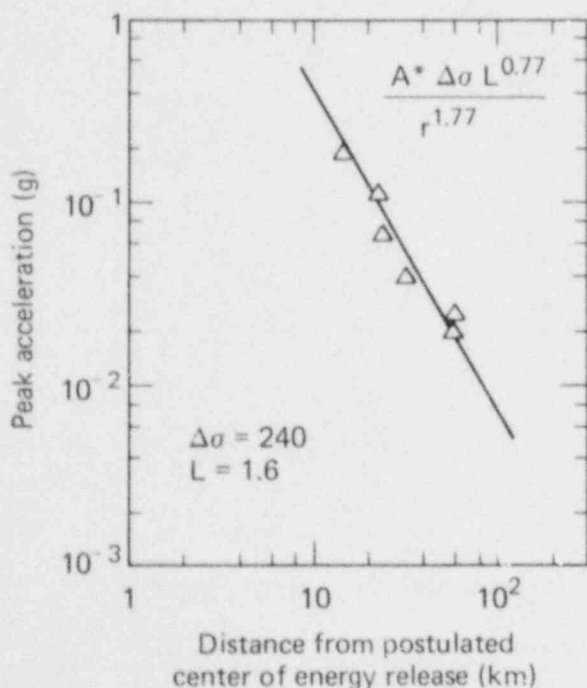


FIG. 21. Fit of Eq. (21) to the acceleration recorded for the Lytle Creek earthquake.

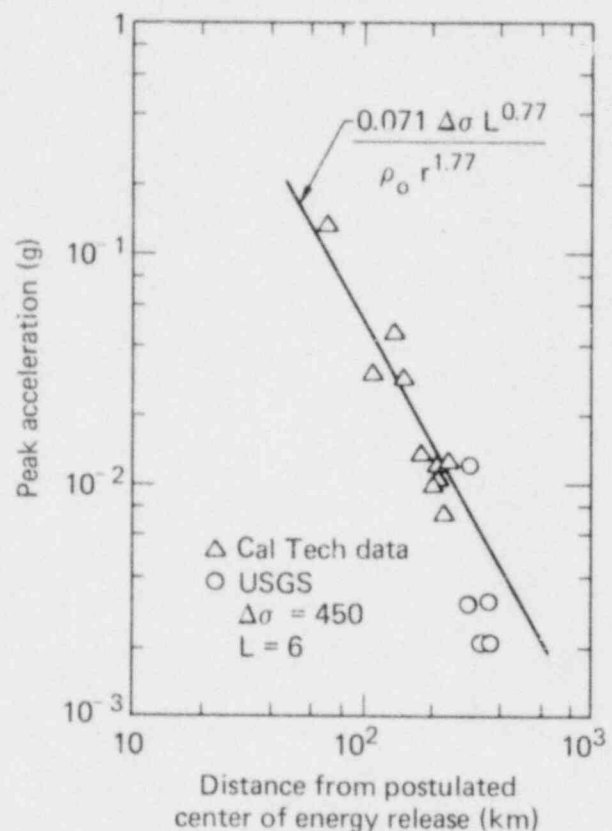


FIG. 22. Fit of Eq. (21) to data from the Borrego Mountain earthquake.

El Centro site; as a result, some tables list 45 km as the distance (e.g., Boore et al.⁷¹). It is also of interest that Heaton and HelMBERGER, modeling the Borrego Mountain earthquake as a radially propagating uniform dislocation confined to a vertical rectangular surface, found their best fit resulted from a fault 11 km long with a stress drop of approximately 500 bars. This is in close agreement with our 450 bars and equivalent radius L of 6 km.

The Parkfield earthquake is an interesting case. The epicenter was located a considerable distance away from the strong-motion array. The aftershock zone suggests that the depth of the focus was between 3 and 13 km. In the near field, it is very important to use the correct value of r in Eq. (21). The correct r is the distance from the center of the nearest region of high stress drop to the recording site. Several possible interpretations of the data exist. For example, Aki⁴⁶ interpreted the Parkfield earthquake in terms of his barrier model. He interpreted the aftershock pattern as the

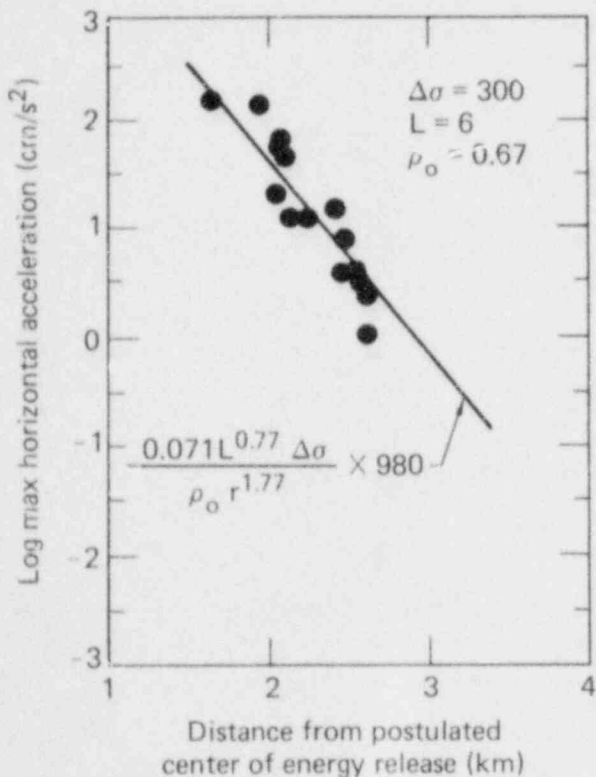


FIG. 23. Fit of Eq. (21) to the recorded peak acceleration for the 1952 Kern County earthquake.

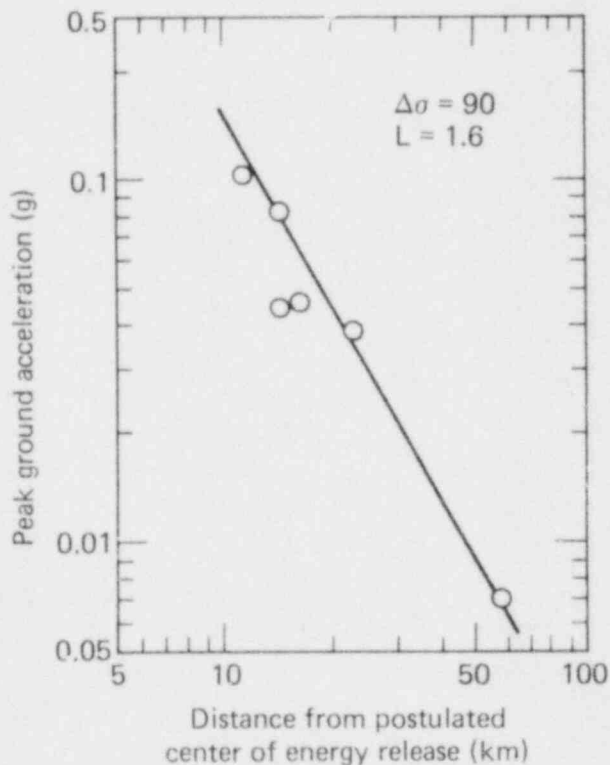


FIG. 24. Fit of Eq. (21) to data from the 1957 San Francisco earthquake.

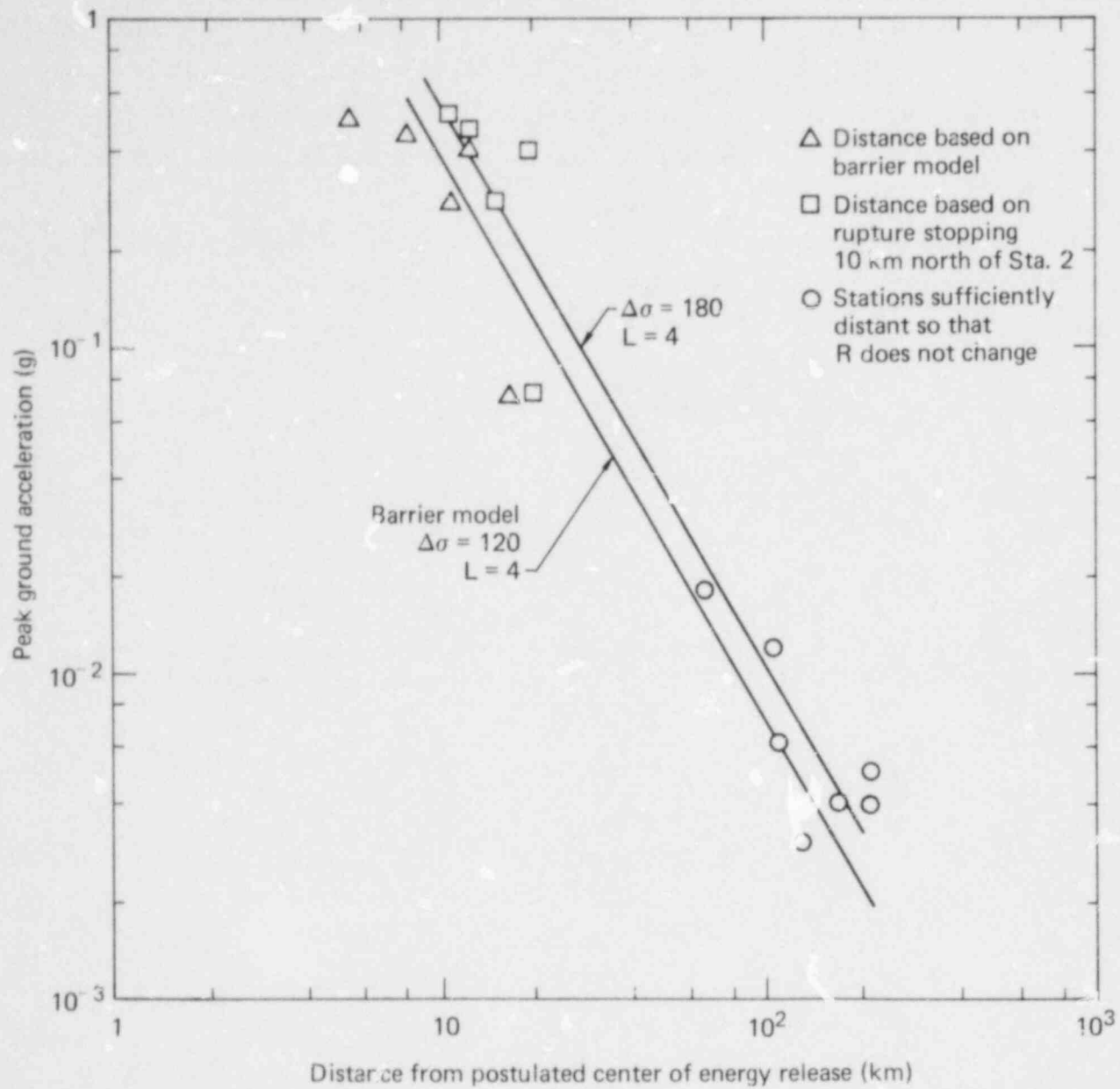


FIG. 25. Fit of Eq. (21) to data from the Parkfield earthquake, using two different locations for the region of high stress drop.

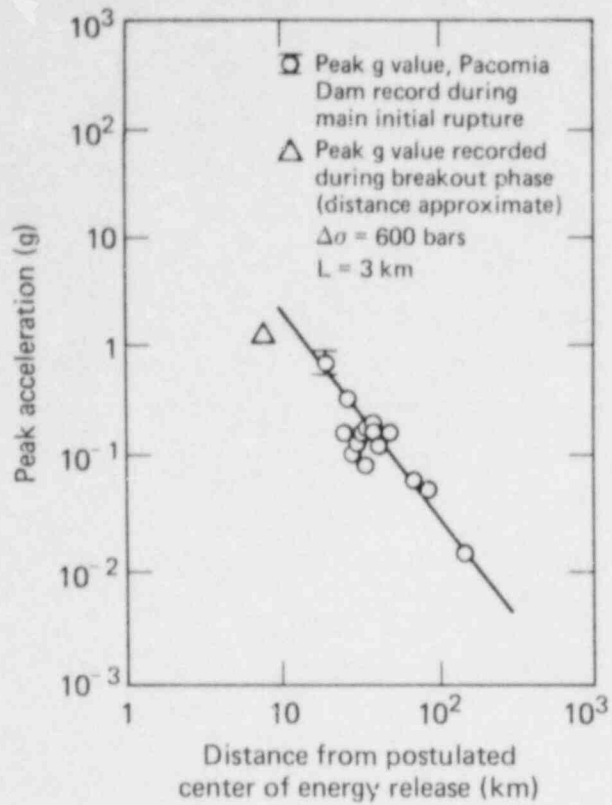


FIG. 26. Fit of Eq. (21) to the recorded peak acceleration for the San Fernando earthquake (data from rock sites only).

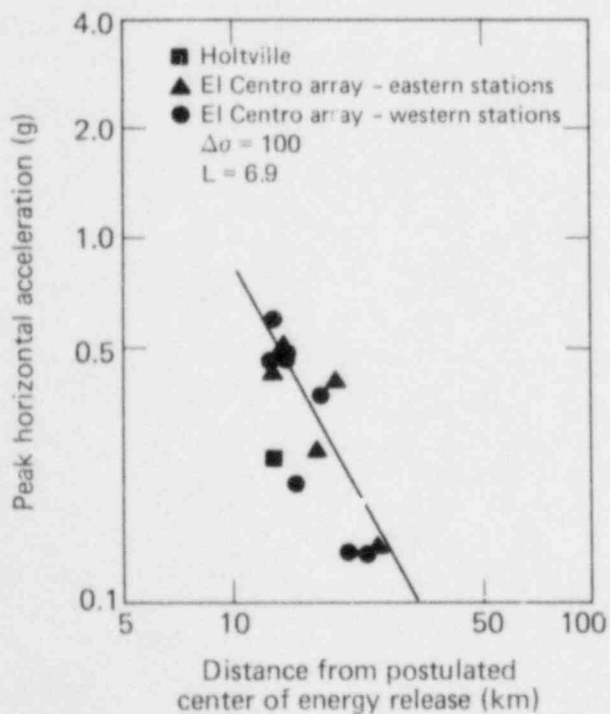


FIG. 27. Fit of Eq. (21) to data from the October 1979 Imperial Valley earthquake, El Centro array.

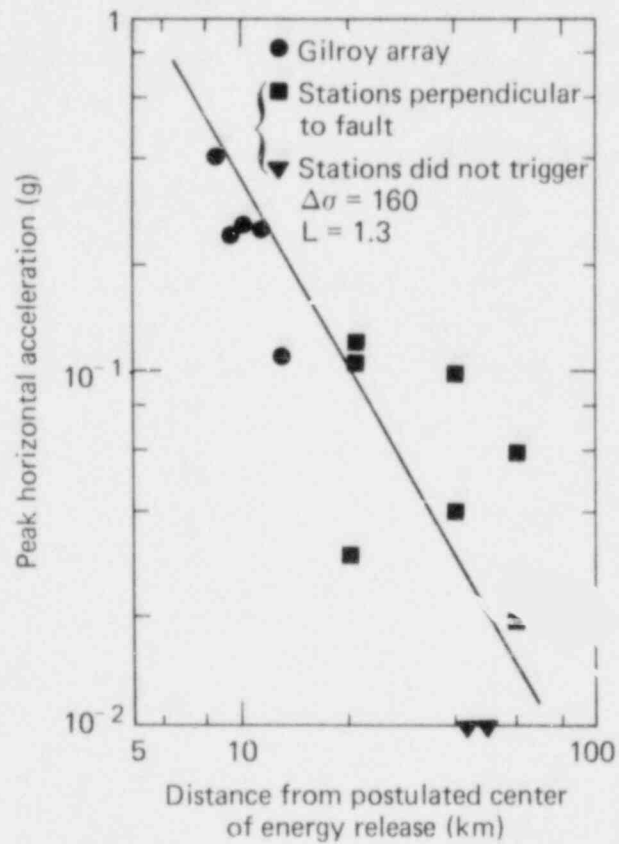


FIG. 28. Fit of Eq. (21) to data from the August 1979 Coyote Lake earthquake.

result of a barrier near the bend in the fault shown in Fig. 29 and argued that the strong ground motion observed at station 2 was from the slipped zone southeast of the barrier. He estimated that the size of the zone was approximately a circle of radius 3 km. We estimate the depth of the center of energy release as about 5 km on the basis of Aki's interpretation of where the barriers are for this portion of the fault. Using this model we obtain $L \sim 4$ km and $\Delta\sigma \sim 120$ bars, in reasonable agreement with Aki's estimate of $L \sim 3$ km and $\Delta\sigma \sim 50$ bars. Aki's estimate of the stress drop was based on his estimate of the average dislocation for this portion of the fault. Figure 26 shows the fit of Eq. (21) for our estimates of $\Delta\sigma$ and L from the Fourier spectrum recorded at the town of Temblor.

Several studies⁷²⁻⁷⁴ of the strong ground motion recorded by the strong-motion array conclude that significant faulting stopped about 20 km southeast of the epicenter rather than in the vicinity of the strong-motion array. If this is the case, i.e., if the region of high stress drop was not

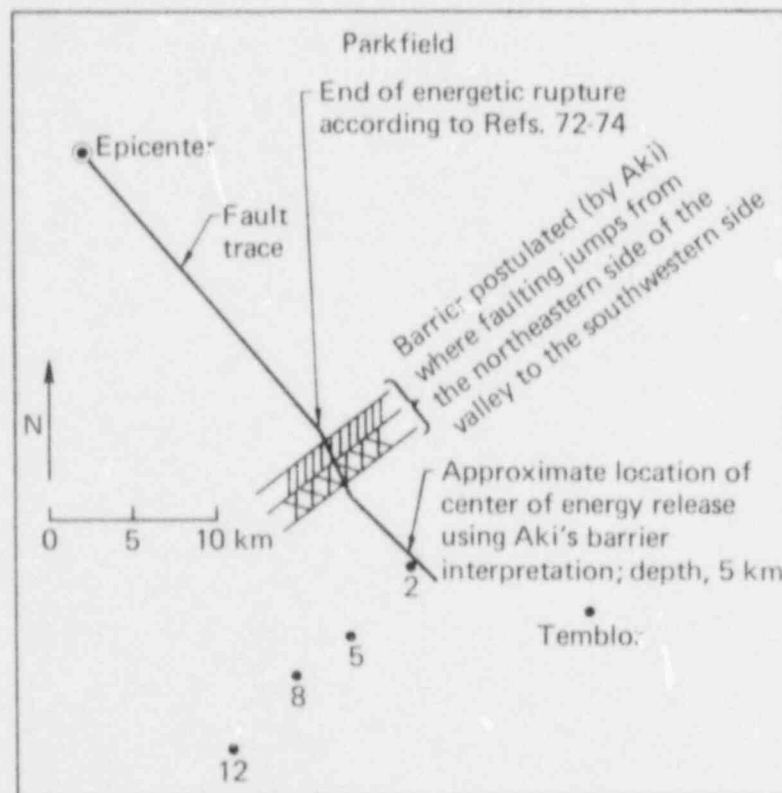


FIG. 29. San Andreas fault near Parkfield, showing recording stations and trace fault.

so close to Station 2, but about 10 km closer to the epicenter, we find $\Delta\sigma = 180$ bars. The fit of Eq. (21) to the data--assuming that the closest highly stressed region is located 10 km north of station 2--is also shown in Fig. 25. In this case, the fit of both the near-source and far-field data is somewhat better.

If Aki's interpretation is correct, then we see from Fig. 25 that departure from Eq. (21) occurs (at least for one earthquake) at

$$r/2L \sim 1 . \quad (23)$$

In Eq. (23) we use $2L$ because the scale length L we used for earthquakes was the equivalent radius, whereas the L for salvo explosions, discussed earlier, was the total length of the line source. Recall that for line-source explosions the data supported an $r/L \sim 1/4$ (where L is the length of the explosive time source).

The San Fernando earthquake is also interesting, as it provides us with one of the few near-source recordings. In Table 4 we used the values of r , $\Delta\sigma$, and L obtained by Trifunac.⁶⁶ Since then, Hanks⁷⁵ has made a very careful study and relocated the hypocenter. Hanks's analysis showed that the initial rupture area was located about 19 km from the Pacoima Dam accelerogram and had a source dimension L between 3 to 6 km and a stress drop between 350 bars (6 km of rupture) and 1400 bars (3 km). In addition, his analysis suggests that the majority of the energy was released in the initial rupture. The peak g value of 1.25 recorded at about 7.7 seconds is interpreted by Hanks as a combination of the arrival of the breakout phase with other wave arrivals. Hanks's results are in general agreement with those of a number of other investigators (e.g., Refs. 76 and 77).

Several values of stress drop and length were used in Eq. (22); in Fig. 19 the predicted spectrum is compared to the spectrum computed from the record at Griffith Park Observatory. It is seen that $\Delta\sigma = 600$ bars and $L = 3$ km in Eq. (22) fit the actual spectrum somewhat better than the other choices shown. Figure 26 shows the comparison of the predicted values of acceleration using Eq. (21) and $\Delta\sigma = 600$, $L = 3$ to the recorded values at rock sites. It is seen that the fit is good. Two values of peak acceleration are plotted for the Pacoima Dam station. One is the peak acceleration recorded during the initial energy release and the other is the peak of 1.25 g that occurred later in the record. As noted above, Hanks found that the majority of the energy

was released in the initial faulting. We feel that the peak g value recorded in the initial shear wave train is the appropriate value for comparison in our model, as the spectrum recorded at 35-45 km used in our estimation of the stress drop should primarily reflect this initial major energy release. The peak of 1.25 g recorded at the Pacoima Dam is a combination of several late arrivals that would not necessarily fall on the predicted curve.

If Trifunac's⁶⁶ estimate of $\Delta\sigma = 100$ bars and $L = 10$ km had been used in Eq. (21), the predicted line would have passed through the 1.25- g point parallel to the line shown. In this case, the estimated curve gives a poor fit to the data.

The recent Imperial Valley⁷⁸ and Coyote Lake⁷⁹ earthquakes of 1979 provide a number of near-source ground-motion records. To apply Eqs. (21) and (22) to the earthquakes we need to know the location of the regions of high stress drop that control the ground motion at the various recording sites. Once r is known, $\Delta\sigma$ and L are easily obtained by fitting Eq. (22) to the recorded Fourier spectra of the ground acceleration. Our analysis of the Parkfield and San Fernando data shows the importance of having a reasonable estimate of r . It also shows that using either the distance from the recording site to the fault or the epicentral distance as an approximation for r can lead to significant error and confusion in understanding the ground motion.

To establish the location of regions of high stress drop and/or possible barriers requires extensive modeling studies well beyond the scope of this report. What follows is a very simplistic analysis of these two events in the framework of our model. A frequent problem in establishing the location of the source of the strong ground motion at a site is the lack of any absolute time in the records. Normally, all that is available is the time difference between the triggering of the instrument and the arrival of the strong S waves. However, for the October 1979 Imperial Valley Earthquake, absolute time was recorded on the El Centro array. This absolute time can be used to help establish for these stations where the seismic energy recorded was generated. Complexities in travel paths and P-S conversions make it difficult to draw direct conclusions from arrival times. These complexities and the still-preliminary nature of the data we are using should be kept in mind when the results of our analysis are assessed.

There are several possible locations for the source of the strong ground motion recorded by the El Centro array. Figure 30 shows the location of the

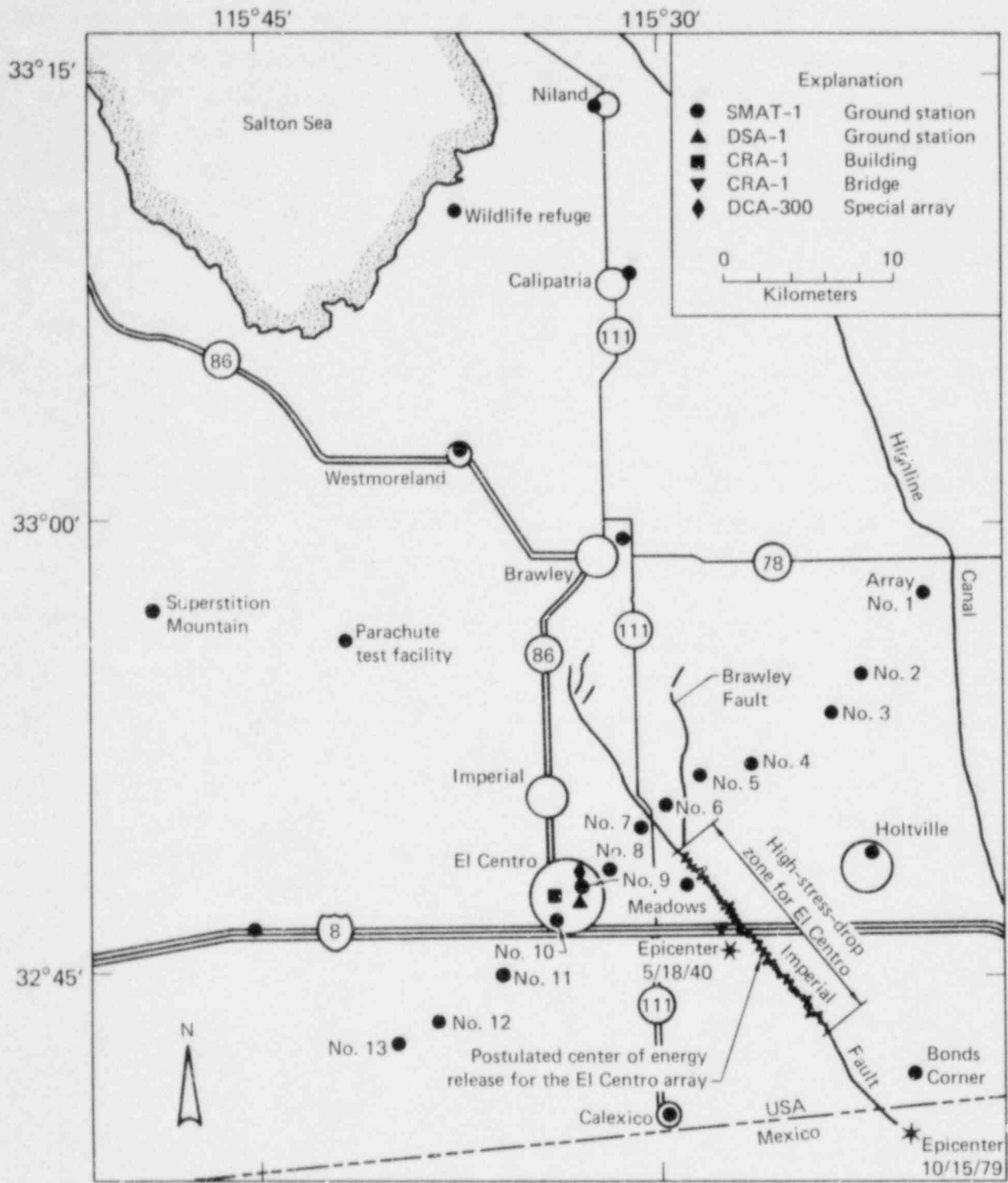


FIG. 30. Strong-motion stations in the Imperial Valley, California.

various stations with respect to the fault. The relative simplicity of the strong-ground-motion pulse at station 7 suggests that the main zone of energy release recorded there was very near. If so, the S waves should have arrived at, say, Station 11, some 13 km away from the fault, about 3-4 seconds later than at Stations 6 and 7 and some 5-6 seconds later (relative to Stations 6 and 7 and about 2 seconds later relative to Station 11) at Station 13, 22 km from the fault. In fact the waves arrived much earlier at these stations, as shown in Fig. 31. Absolute time is not available for Station 7; therefore, to avoid assumptions about when Station 7 started recording, we have used Station 6 (Fig. 31), for which absolute time is available. The tentative arrival times at the various stations in the array are given in Table 8. We have assumed that the start time for Station 7 was the same as for Station 8.

TABLE 8. Arrival times of S wave at the stations of the El Centro array, distances, and peak ground motion.

Station No.	Start time ^a	Δt of S wave after start	Actual arrival time	Distance from fault (km)	Distance from postulated zone of high stress drop (km)	Peak horiz. accel. (cm/s ²) ^b	Peak horiz. velocity (cm/s) ^b
6	17:01	4.0	17:05	1	13	424	109
8	17:00	5.0	17:05	4	13	598	53
5	17:01	4.0	17:05	4	14	517	87
4	17:01	4.0	17:05	7	14	483	78
11	17:00	6.0	17:06	13	17	374	39
2	17:01	6.0	17:07	16	19	405	31
12	17:01	6.0	17:07	18	21	139	19
13	17:02	5.0	17:07	22	24	136	15
1	17:02	6.0	17:08	22	25	140	15
7	--	4.5	?	1	13	453	108
Diff. array	--	5.0	?	5	14	477	68
10	--	5.0	?	9	15	221	44
3	--	5.5	?	13	17	261	46

^aPorcella et al.⁷⁸

^bFrom plots of corrected data from tape.

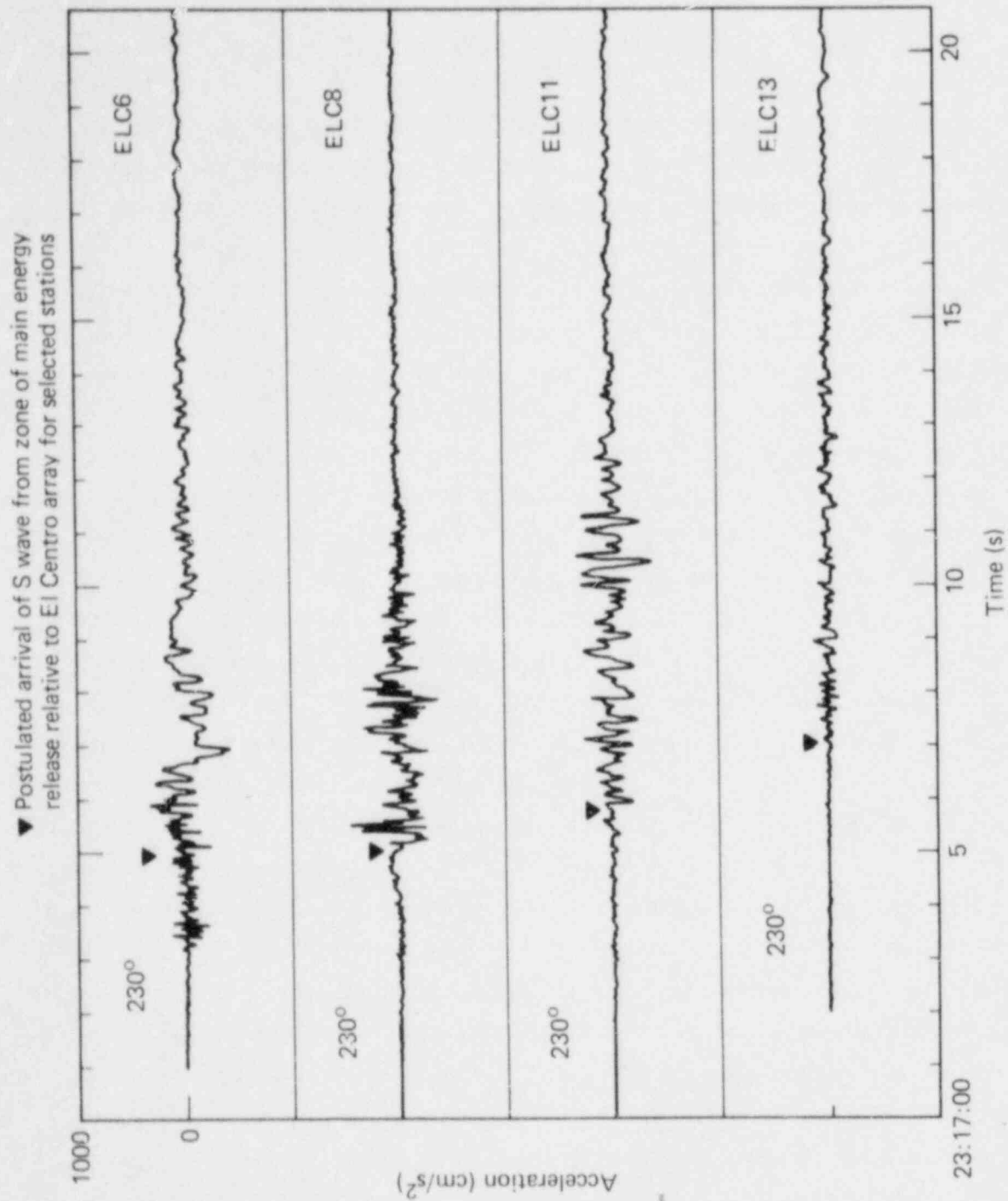


FIG. 31. Postulated arrival times of S wave at selected stations of the El Centro array.

As can be seen from Table 8, the S waves arrive very early at all stations relative to Stations 6 and 7, which are very near the fault. This suggests that the seismic energy was generated at some distance from these stations. A reasonable location for a barrier (or region of high stress drop) is the region where the Brawley fault joins the Imperial Valley fault. The preliminary epicenter location map⁸⁰ shows a large number of aftershocks in this zone, suggesting that it may be a major barrier. This would put the end of the rupture zone about 3-5 km southeast of Station 7 along the fault. The equivalent radius of this zone is estimated by use of Eq. (22) at about 7 km. Thus the center of the zone is about 10 km southeast of Station 7. In addition, the center of the zone of high stress drop must be located at a depth of at least 7-8 km. This would put the beginning of the zone of high stress drop at a depth of at least 14 km and at a distance of 14 km southeast of Station 7. Station 13 is about 28 km from this location and Station 7 about 20 km. The energy would arrive at Station 7 approximately 2 seconds before arriving at Station 13, in reasonable agreement with the observed data.

We fitted Eq. 22 to the Fourier spectra recorded at several stations and found $\Delta\sigma = 100$ and $L = 6.9$ km for the center of the main source of energy release relative to the El Centro array located 10 km southeast of Station 7 at 8 km depth. The fit of Eq. (22) to the spectrum of the ground motion from Station 8 is shown in Fig. 20. It is difficult to obtain a good estimate of the parameter L because the time history from which the spectrum was computed was filtered with a ramp filter starting at 5.9 seconds and ending with zero amplitude at 38 seconds. The filtered region is shown in Fig. 20. It can be seen from this figure that the filtering makes it very difficult to estimate L . This is typical of all the El Centro stations: our fit seems reasonable but is difficult to confirm. In Fig. 27 we have plotted the peak horizontal ground acceleration recorded at the various stations making up the El Centro array. We also show in Fig. 27 the fit of Eq. (21) to the data using our location and our values of $\Delta\sigma = 100$ and $L = 6.9$ in Eq. (21). Equation (21) fits the data reasonably well. We have not plotted data other than from the El Centro array and Holtville, as they could also be influenced by other regions of high stress drop or other barriers. The ground acceleration recorded at Holtville appears low compared to that at the El Centro array. This could be due to directivity effects from the rupture propagating northward away from Holtville or to local site effects.

It is of some interest to contrast the El Centro array with the Parkfield array. One problem is that absolute time is not available for the Parkfield array, making any interpretation suspect. For the Parkfield array, Station 5 was approximately 5.4 km from the fault and Station 2 was 0.2 km. If Aki's model⁴⁶ (which puts the center of energy release very near Station 2--we located it at a depth of approximately 5 km and about 2 to 3 km northwest of Station 2) is accurate, we would expect the S waves to arrive at Station 5 about 1 to 2 seconds later than at Station 2. If we assume that both instruments were triggered at about the same time, as at El Centro, this is about the difference in arrival times of the S wave observed from the recorded data at Stations 2 and 5. We cannot verify this conclusion using the more distant stations at Parkfield, as either they triggered at later times than Stations 2 and 5 or Station 5 triggered very early and the others at the same time, which would place the center of energy release back near the bend in the fault.

Absolute times are not available for the Coyote Lake earthquake⁷⁹; hence other reasoning must be used to locate the center of energy release relative to the Gilroy array. Due to the relative simplicity of the recordings at Station 6 of the Gilroy array, however, the center of energy release should be close to Station 6. If we interpret the aftershock pattern of the Coyote Lake earthquake in terms of Aki's barrier model, similarly to that of the Parkfield earthquake, we can see an interesting change in aftershock alignment southeast of Station 6 as compared to that northwest of Station 6. Figure 32 shows our simplistic model near Station 6. If we assume that most of the instruments in the Gilroy array were triggered at about the same time, we can analyze arrival times. Station 2 recorded a strong signal and a P-wave train about as strong as recorded at Stations 6 and 4. If Station 2 started about the same time as Station 6 and if we assume that the center of energy release was near Station 6, then because Station 2 is about 7 km from the fault we would expect the waves to arrive at Station 2 about two seconds after they arrive at Station 6. They appear to arrive closer to 1 second. This could be due to different start times; however, if the depth of energy release is at approximately 10 km and 2-3 km northwest of Station 6 on the fault, then the distance to Station 2 is about 11 km and to Station 6 about 8 km, and we would expect the difference in arrival time to be about 1 second.

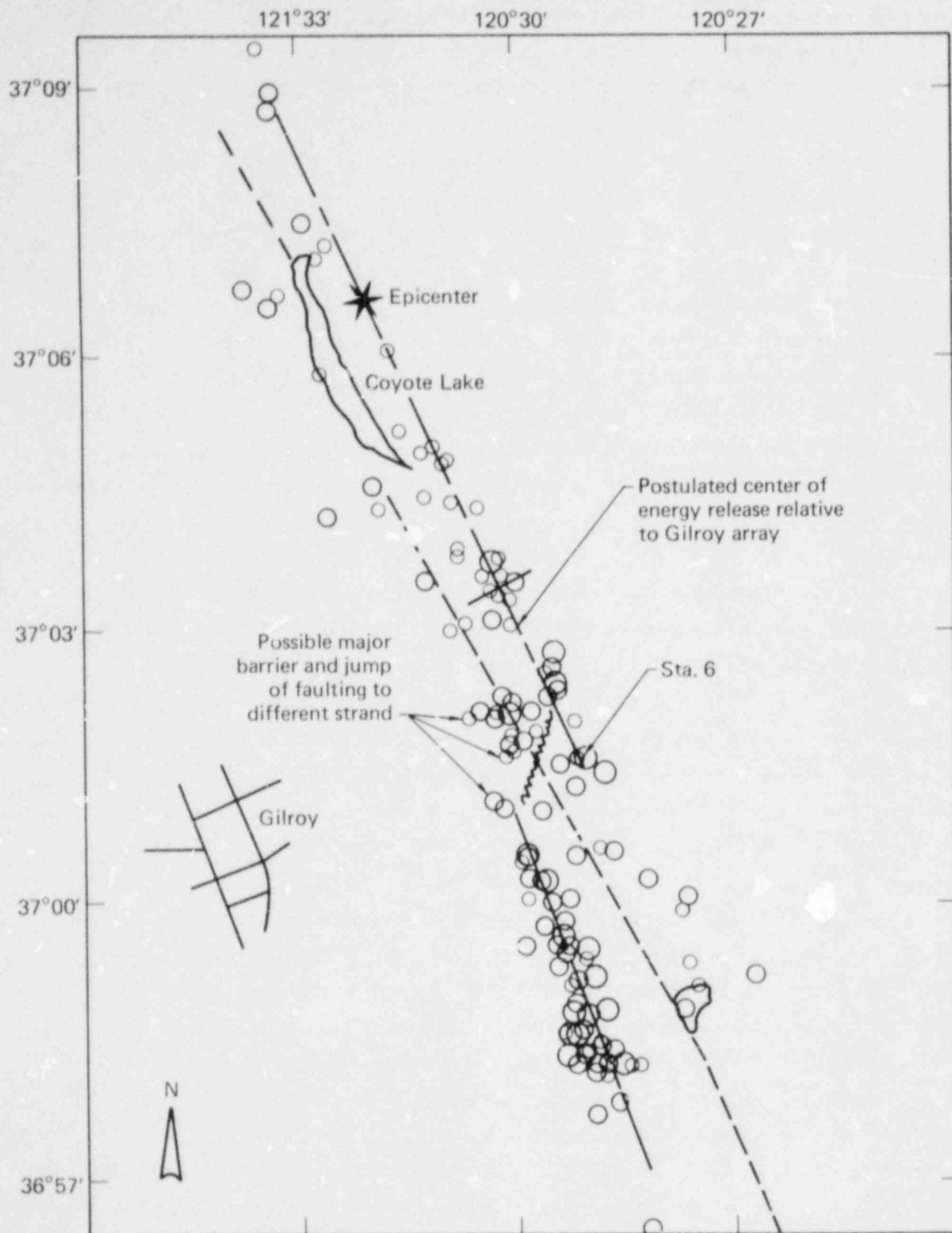


FIG. 32. Location of the epicenter of the Coyote Lake earthquake, main shock and aftershocks.

Our tentative location of the center of energy release for the Gilroy array is shown in Fig. 32. We assume that it is located at a depth of 5-10 km, and chose 8 km as a reasonable value based on the above analysis of arrival times. We show the data from the Gilroy array as well as from the stations more or less perpendicular to the fault. We felt that stations located at both the north and south ends of the fault could be influenced by barriers at both ends, and hence did not include them in the plotted data. Also shown in Fig. 28 is the fit of Eq. (21) to the data for $\Delta\sigma = 160$ bars and $L = 1.3$ km. These values were obtained by fitting Eq. (22) to the Fourier spectra computed from the data recorded at several stations of the Gilroy array. Equation (21) seems to fit the data reasonably well. There seems to be considerable scatter to the data from the Coyote Lake earthquake, suggesting the occurrence of complex processes; simple models will thus not capture all aspects of the observed ground motion.

Further verification of our model can be obtained by comparing the recorded peak velocity with that predicted by the proposed methodology; i.e., by combining the scaling relation, Eq. (12), with

$$v^*(r^*) = B^*/(r^*)^m$$

to get

$$v_{\text{recorded}} = \frac{B^* \Delta\sigma L^m}{r^m} \left(\frac{\beta}{\mu}\right)^*, \quad (24)$$

where B^* and m are constants. The difficulty is in determining B^* and m . It is not possible to determine B^* and m in the same manner as we found A^* and m above because the peak velocity is associated with much longer-period waves than the peak acceleration; hence the recorded peak velocities of the aftershocks are a combination of the seismic energy of the aftershock and oscillations (not yet damped out) of the preceding events. By examining explosion data and a few earthquakes we determined that a value of $m = 1.66$ gives a good fit of both near-source and far-field velocity data. This value was used and the value of B^* was determined by an "eyeball" fit of Eq. (24) to the data from San Fernando to obtain

$$v = \frac{1.2 \Delta\sigma L^{1.66}}{r^{1.66}} \left(\frac{\beta}{\mu}\right)^* \quad (25)$$

Figures 33-36 show the fit of Eq. (25) to the recorded velocity data from four of the earthquakes in Table 7. The fit is reasonable, although the velocity data are much less reliable than acceleration data. Not enough velocity data were available from the other earthquakes to make meaningful comparisons. The model did fit what few data were available, except for the Coyote Lake earthquake, where the predicted results were low by about a factor of 2. Corrected points were plotted in a few cases when the peak velocity occurred very late in the record and appeared to be related to the filtering problem discussed by Hanks.⁸¹

We conclude that the reasonable fits to the data verify our scaling rules, Eqs (11)-(13), and our resultant model, Eqs. (21) and (25), even in the near-source region. Only when the local center of energy release is very shallow and directly under the site of interest will there be significant departures from the attenuation given by Eq. (21). Because the ground motion attenuates as $1/r^{1.8}$, it is important to account for distance effects when comparing ground motion from different earthquakes.

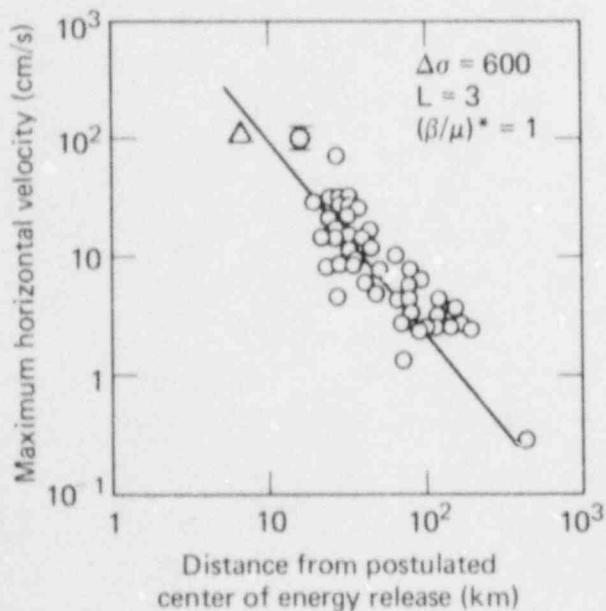


FIG. 33. Fit of Eq. (25) to the peak velocity recorded for the San Fernando earthquake.

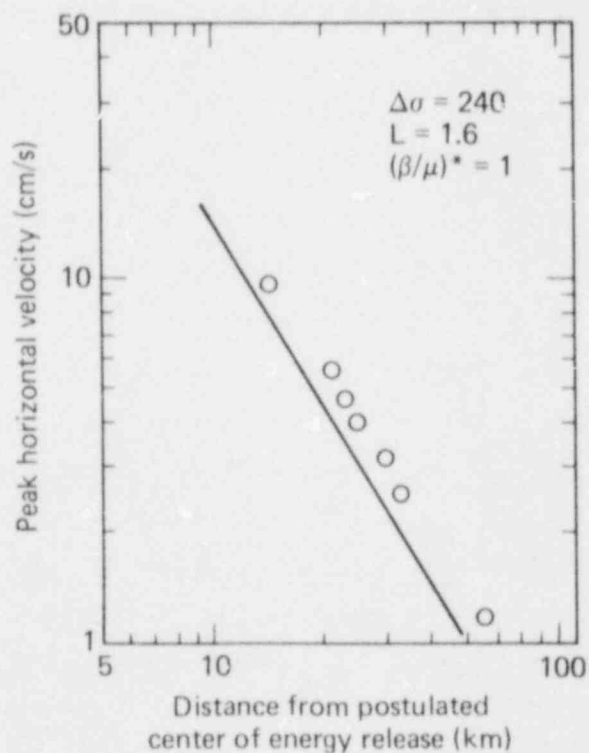


FIG. 34. Fit of Eq. (25) to the data recorded from the Lytle Creek earthquake.

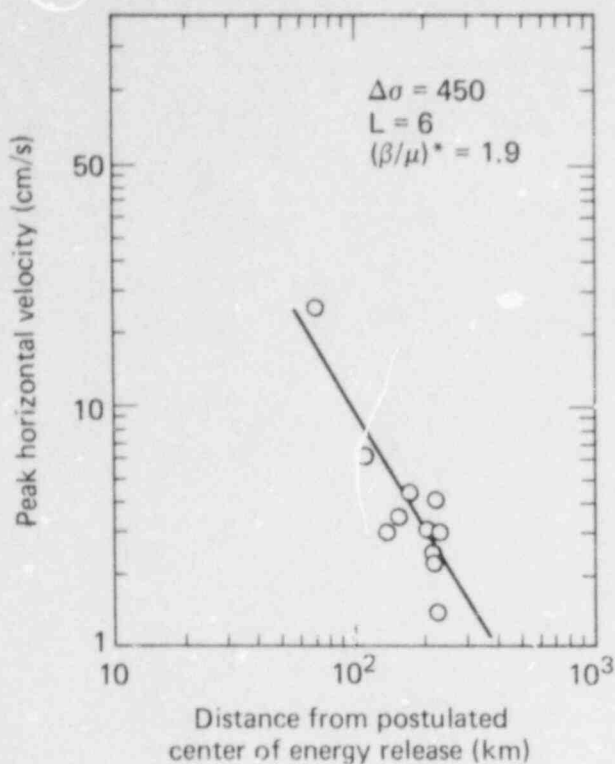


FIG. 35. Fit of Eq. (25) to the data recorded from the Borrego Mountain earthquake.

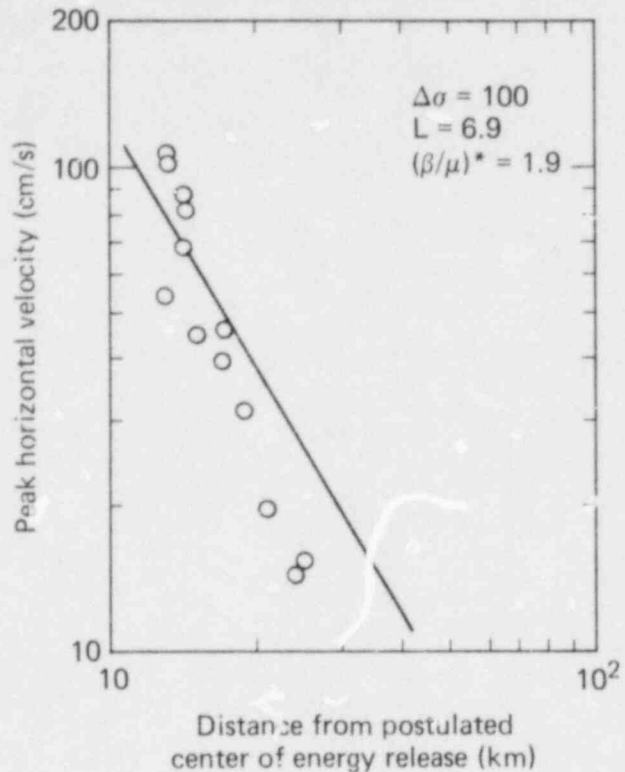


FIG. 36. Fit of Eq. (25) to the peak velocity recorded at the El Centro array, Imperial Valley earthquake, October 15, 1979.

THE ROLE OF MAGNITUDE

As noted in the Introduction, the only parameter of an earthquake often available is magnitude. It is therefore useful to be able to express our Eqs. (21) and (25) in terms of M_L . To do this we need a relation between M_L , $\Delta\sigma$, and L . Thatcher and Hanks⁸² derived such a relation in the far field, using the shape of the far-field displacement pulse on which Brune's model is based, and computed the approximate maximum trace amplitude in the Wood-Anderson seismogram. Although we have used Brune's model to determine $\Delta\sigma$ and L , these quantities are in fact spectral shape parameters. $\Delta\sigma$ is effectively the envelope of the maximum of the spectral amplitudes of the Fourier amplitude spectrum of the acceleration and L is really the corner frequency. Using these two empirically determined parameters, it is possible to model many of the essential features of the Fourier amplitude spectrum of the recorded ground acceleration by use of Brune's far-field model. The work

of Kanamori and Jennings⁸³ shows that M_L can be determined from the recorded ground acceleration. Thus it seems reasonable to assume that M_L is related directly to $\Delta\sigma$ and L , as these two parameters control the peak ground motion. To get the desired relation we first note that^{22,23}

$$M_L = \log A - \log A_0 ,$$

where

A = a constant proportional to the maximum response of a Wood-Anderson seismometer,

$-\log A_0$ = a factor defined by Richter and shown by Trifunac¹ to be approximately $1.4 + \frac{r}{50}$ for $r < 70$ km.

We assume that A is proportional to the Fourier amplitude spectrum of the ground displacement at $T_s = 0.8S$. Using $\log A$ from Eq. (22), we obtain

$$M_L \sim K + \log \Delta\sigma + \log L - \log \left(\frac{1}{T_s^2} + f_c^2 \right) - \log r - \log A_0 . \quad (26)$$

The term $(-\log R - \log A_0)$ in Eq. (26) is approximately constant for distances r between 10 and 50 km (with a maximum variation of about 0.2 units) and between 5 and 70 km (about 0.5 units). Making this approximation and substituting for T_s and β , we get

$$M_L = K_1 + \log \Delta\sigma + G(L) ,$$

where $G(L) = \log L - \log \left(1.56 + \frac{1.7}{L^2} \right)$.

The term $G(L)$ varies approximately (with an error less than 0.1 magnitude) as

$$G(L) \sim 1.5 \log L + C, \quad 0.5 < L < 15 \text{ km}$$

and as

$$G(L) \sim 2.3 \log L + C, \quad L < 0.5 \text{ km} .$$

Hence

$$M_L \sim K + \log \Delta\sigma + 1.5 \log L, \text{ where } 0.5 \leq L \leq 15, \quad (27)$$

and

$$M_L \sim K + \log \Delta\sigma + 2.3 \log L, \text{ where } L < 0.5. \quad (28)$$

Our result is the same as that derived by Thatcher and Hanks,⁸² although our values of $\Delta\sigma$, L , and the constant K are different. Thatcher and Hanks's values are determined from far-field data, and hence represent averages over the fault, whereas ours are determined from the high-frequency part of the spectrum and represent local regions of high stress drop. For smaller earthquakes we might expect $\Delta\sigma$ and L to be the same as both near-source and far-field spectra, representing the average over the small region of rupture. Certainly as the earthquake becomes very large we would expect a variation of stress drop along the rupture zone, and hence far-field and near-source determinations of the parameters $\Delta\sigma$ and L might well be significantly different. Typically for large events our values for L are smaller than those obtained from the far-field data and our values of local stress drop are much larger than typical static values averaged over the entire rupture area of the fault.

To test the applicability of Eq. (27), we fit the relation

$$M_L = C_1 + C_2 \log \Delta\sigma + C_3 \log L$$

to the combined data in Tables 4, 5, and 7 (except for the Coyote Lake and Imperial Valley earthquakes) and found

$$M_L = 3.5 + 1.5 \log L + 0.9 \log \Delta\sigma, \text{ where } \sigma = 0.15,$$

which is in reasonable agreement with Eq. (27). We excluded the Coyote Lake and Imperial Valley earthquakes because M_L has not yet been computed from strong-motion data consistent with the other earthquakes in Tables 4, 5, and 7.

As is evident from these tables, stress drop varies more than the parameter L , which is related to the corner frequency of the spectrum. One

could solve for $\log L$ in terms of M_L and $\log \Delta\sigma$ from Eq. (27), or regress the data in the form

$$\log L = C_1 + C_2 M_L + C_3 \log \Delta\sigma .$$

However, in view of the number of approximations that have been introduced, the results given in Eqs. (27) and (28) are not of sufficient quality to warrant such elaborate model building. The results, while not quantitatively reliable, provide a useful qualitative insight into the relation between the peak-ground-motion parameters M_L and the key earthquake source parameters. Thus, solving Eq. (27) for $\log L$ and substituting for L in Eqs. (21) and (25), we obtain

$$\log a \sim K_1 + 0.5 \log \Delta\sigma - 1.8 \log r + 0.5 M_L , \quad (29)$$

$$\log v \sim K_2 - 0.1 \log \Delta\sigma - 1.7 \log r + M_L . \quad (30)$$

These equations suggest that peak acceleration is strongly influenced by both magnitude and stress drop, whereas the peak velocity is strongly related to earthquake magnitude. It must be kept in mind that site effects are not included in Eqs. (29) and (30). Site factors have been shown to introduce considerable variation in both the recorded peak ground velocity and acceleration.

Eqs. (29) and (30) suggest that peak velocity should correlate more strongly with earthquake magnitude and distance than does peak acceleration. This does not appear to be the case, as the coefficient of variation (C.O.V.) for peak velocity is typically about the same as for peak acceleration. One possible explanation is that several investigators^{19,71} have found that if site type is included in the regression analysis, it is significant only for peak velocity and not for peak acceleration.^{2,14,19} Thus the large C.O.V. observed in typical correlations between v , M , and r may be due primarily to site effects, and the large C.O.V. observed in typical correlations between a , M , and r may be due to variations in $\Delta\sigma$ and L .

DISCUSSION OF RESULTS

Equation (21) not only verifies Hanks and Johnson's⁴ conclusion that the peak g value recorded is not a function of earthquake magnitude alone, but also gives a method to predict the peak g value expected from an earthquake once the source parameters $\Delta\sigma$ and L as well as the distribution of zones with large $\Delta\sigma$ are known. We have chosen to interpret $\Delta\sigma$ in terms of stress drop. In fact the parameter actually measured is a smoothed estimate of the peak amplitude of the Fourier spectrum of the measured ground acceleration corrected for attenuation. For most of the earthquakes considered in this report, $\Delta\sigma$ is a measure of the amplitude of higher-frequency radiation. Studies by a number of investigators show that the emission of significant amounts of high-frequency energy is caused either by sudden changes in rupture velocity, or in the levels of σ_U , σ_T , or σ_F , or by variations in $\sigma_U - \sigma_F$ or $\sigma_T - \sigma_F$. Without detailed modeling, an examination of the Fourier amplitude spectrum does not disclose which mechanism was the most important--in fact, even detailed modeling is unlikely to sort out the various possible factors. Thus, for simplicity, we have lumped all such factors together under dynamic stress drop.

The same sort of discussion applies to the parameter L . In our model L is clearly a direct measure of the corner frequency. Physically it is some measure of the size of the zone that is contributing most significantly to the radiation of frequencies higher than the corner frequency. For example, if the cause of high-frequency radiation is the sudden stopping or starting of the rupture because of a barrier, L would be a measure of the size of the barrier. If, on the other hand, the high-frequency radiation is due to the existence of a significant zone with change in $\sigma_U - \sigma_F$, or in the parameter $S = (\sigma_U - \sigma_T) / (\sigma_T - \sigma_F)$ defined by Das,⁴⁶ L would be a measure of the size of this zone. In actual fact, depending on how far away the recording station is from the zones along the fault of interest, L and $\Delta\sigma$ often will be an averaged measure of several such zones.

We noted earlier that the stress drops obtained using near-source data are generally significantly larger than those obtained in the far field from the seismic moment, as the former measure locally high dynamic quantities and the latter are a measure of an averaged $\Delta\sigma$ over the entire fault rupture zone. The two quantities are different. To highlight this, we call the

parameter $\Delta\sigma$ determined from near-source data the "dynamic stress drop" and the parameter $\Delta\sigma$ determined from far-field data the "static stress drop." Care must be taken not to intermix them in various relations.

Equations (21) and (25) can be used to make estimates of the expected peak ground motion at a site for an earthquake with given source parameters. As noted above, the values of the stress drop and length should be consistent with those calculated from near-source data. There appear to be upper limits to the stress drop that limit the value of peak acceleration; however, it is evident that large peak-g values could be observed from any magnitude earthquake for large enough stress drop. Typically, larger earthquakes are associated with larger values of the parameter L . Thus, as seen from Eq. (21), one would expect to observe larger peak ground motions. This, of course, explains why the correlations of magnitude work as well as they do. It also explains the large variation in the recorded data. In addition, it must be kept in mind that larger earthquakes are made up of a number of zones with large $\Delta\sigma$. As discussed above, in the near-source region the peak g value is controlled by the dimension of the nearest region with large stress drop. This can present a problem for large earthquakes, as reasonable values for $\Delta\sigma$ and L are not known (few data exist), nor is the distribution of these zones along the fault. For smaller earthquakes more data exist, and it is possible to obtain reasonable estimates for $\Delta\sigma$ and L for highly seismic regions such as southern California. For larger earthquakes the values of L might be different, not only because of the physical size of the rupture zone but also because several zones of high stress drop may be located close together, and thus the correct value would be some equivalent L for the two zones. The recorded ground motion at Bonds Corner from the recent October 1979 Imperial Valley earthquake may well be an example of the superposition of ground motion from several such zones. Because of the complexity of this record and the lack of data from other nearby stations, we did not attempt to analyze the Bonds Corner record but chose instead to analyze the El Centro array, where a large number of stations were available and the existence of a potential barrier provided a provisional location for the local energy release.

We can use Eq. (29) to make very approximate estimates of the ground motion from earthquakes of various magnitudes. Figure 37 illustrates typical and upper-limit ground motion that might be expected from such earthquakes. For typical cases a stress drop of about 100 bars seems average and 1000 bars

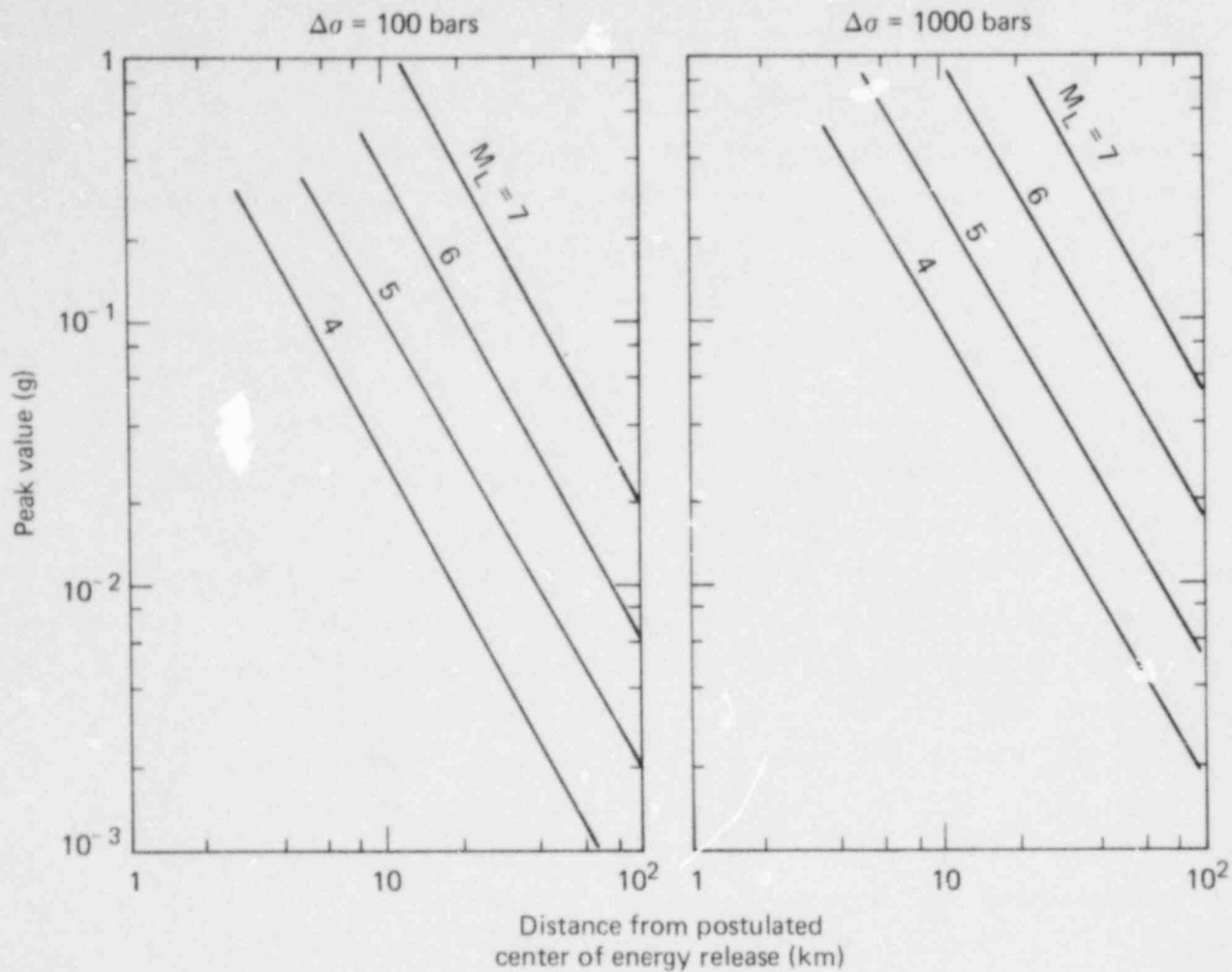


FIG. 37. Estimated peak g value of earthquakes of various magnitudes for two values of stress drop.

seems to be an upper limit, although there is no evident physical reason for this. As discussed above, Fig. 37 may be somewhat misleading for large-magnitude earthquakes, as the estimates shown assume that only one region of high stress drop was involved. There will often be several such regions, so that a much larger area than is suggested by Fig. 37 would experience strong ground motion. There is currently no way to estimate the number of highly stressed regions along the rupturing fault. For estimating the ground motion at a given site the above considerations are not a serious problem, as it is generally assumed that the highly stressed region is at a point on the fault closest to the site. On the other hand, if one were trying to correlate the observed ground motion, then the above considerations would be important.

There are a number of important limitations to the above analysis. The basic form of Eq. (21) is most likely valid, but the constants could be regionally dependent. In addition, in other tectonic settings the difference between strike-slip, thrust, and normal faulting earthquakes may be more important than in California. Very deep earthquakes must also be considered separately.

CONCLUSIONS

Many of the conclusions of this report are not new; however, the scaling rules and Eqs. (21) and (25) do provide a way to relate the ground motion from various earthquakes. The results underscore the conclusion that the energy released from a rupturing fault is highly variable, and that to understand the ground motion recorded at any particular station it is necessary to use the correct distance from the center of the zone of maximum high-frequency energy release near the station and not to approximate this by using the shortest distance to the fault. A few kilometers difference introduces significant differences in ground motion, particularly in the near-source region.

Our results show that Eqs. (21) and (25) can be used to estimate the ground motion very near the fault; however, when $r/L < 1$ then Eqs. (21) and (25) give estimates that are too high. We found that the parameter L is sufficiently small and the center of local energy release sufficiently deep so that Eqs. (21) and (25) are generally valid to within a few kilometers of the fault.

The foregoing scaling rules and equations are based on simplistic concepts, and provide only a first approximation to the ground motion that can be expected from an earthquake with given location and estimated ranges from the key source parameters $\Delta\sigma$ and L . Corrections should be applied to the estimates from Eqs. (21) and (25) to account for any significant site factors and potential for focusing the seismic energy towards the site.

Our results show that peak acceleration is a function of both earthquake magnitude and stress drop, while peak velocity is much more strongly a function of magnitude only. Generally speaking, we would expect larger-magnitude earthquakes to have higher peak accelerations than smaller-magnitude earthquakes because they involve significantly larger regions of dynamic stress drop.

REFERENCES

1. H. Kanamori and D. Anderson, "Theoretical Basis of Some Empirical Relations in Seismology," Bull. Seism. Soc. Am. 65, 1073-1095 (1975).
2. M. D. Trifunac, "Preliminary Analysis of the Peaks of Strong Earthquake Ground Motion - Dependence of Peaks on Earthquake Magnitude, Epicentral Distance and Recording Site Conditions," Bull. Seism. Soc. Am. 66, 189-219 (1976).
3. D. E. Hudson, "Strong Motion Earthquake Measurements in Epicentral Regions," Proc. 6th World Conf. on Earthquake Engineering (New Delhi, 1977).
4. T. C. Hanks and D. A. Johnson, "Geophysical Assessment of Peak Accelerations," Bull. Seism. Soc. Am. 66, 959-968 (1976).
5. N. M. Boore, "Empirical and Theoretical Study of Near Fault Wave Propagation," Proc. 5th World Conf. on Earthquake Engineering (Rome, 1973).
6. O. W. Nuttli, "Seismic Wave Attenuation and Magnitude Relations for Eastern North America," J. Geophys. Res. 78, 876-885 (1974).
7. D. L. Bernreuter, Estimates of the Epicentral Ground Motion in the Central and Eastern United States, Lawrence Livermore National Laboratory, Livermore, California, Preprint UCRL-78369 (to be published in Proc. 6th World Conf. on Earthquake Engineering).
8. N. Ambraseys, "Characteristics of Strong Ground Motions in the Near-Field of Small Magnitude Earthquakes," Proc. 5th Conf. European Committee on Earthquake Engineering (Istanbul, 1975).
9. C. A. Cornell, H. Banon, and A. F. Shakal, "Seismic Motion and Response Prediction Alternatives," Earthq. Eng. Struct. Dynam. 7, 295-315 (1979).
10. N. C. Donovan, "A Statistical Evaluation of Strong Motion Data Including the February 9, 1971, San Fernando Earthquake," Proc. 5th World Conf. on Earthquake Engineering (Rome, 1973).
11. L. Esteva and R. Villaverde, "Seismic Risk, Design Spectra and Structural Reliability," Proc. 5th World Conf. on Earthquake Engineering (Rome, 1973).
12. I. M. Idriss, "Characteristics of Earthquake Ground Motions," paper presented at the Specialty Conf. on Earthquake Engineering and Soil Dynamics, ASCE, Pasadena, California, June 19-21, 1978.

13. R. A. Johnson, "An Earthquake Spectrum Prediction Technique," Bull. Seism. Soc. Am. 63, 1255-1274 (1973).
14. R. K. McGuire, "Seismic Ground Motion Parameter Relations," J. Geotech. Engr. Div., Proceedings of the American Society of Civil Engineers 104, 481-490 (1978).
15. R. K. McGuire, "A Simple Model for Estimating Fourier Amplitude Spectra of Horizontal Ground Acceleration," Bull. Seism. Soc. Am. 68, 803-822 (1978).
16. J. R. Murphy and L. J. O'Brien, "The Correlation of Peak Ground Motion Acceleration Amplitude with Seismic Intensity and Other Physical Parameters," Bull. Seism. Soc. Am. 67, 877-915 (1977).
17. D. L. Orphal and J. A. Lahoud, "Prediction of Peak Ground Motion from Earthquakes," Bull. Seism. Soc. Am. 64, 1563-1574 (1974).
18. M. D. Trifunac, "Preliminary Empirical Model for Scaling Fourier Amplitude Spectra of Strong Ground Acceleration in Terms of Earthquake Magnitude, Source-to-Station Distance and Recording Site Conditions," Bull. Seism. Soc. Am. 66, 1323-1324 (1976).
19. Shannon & Wilson, Inc. and Agbabian Associates, Statistical Analysis of Earthquake Ground Motion Parameters, USNRC Report NUREG/CR-1175 (1979).*
20. N. N. Ambraseys, "Maximum Intensity of Ground Movements Caused by Faulting" Proc. 4th World Conference on Earthquake Engineering 1, p. A-2-154 (1969).
21. J. A. Blume, "Earthquake Ground Motion and Engineering Procedures for Important Installations Near Active Faults," Proc. 3rd World Conf. on Earthquake Engineering IV, 53-57 (New Zealand, 1965).
22. B. Gutenberg and C. F. Richter, "Earthquake Magnitude Intensity, Energy and Acceleration," Paper 1, Bull. Seism. Soc. Am. 32, 163 (1942).
23. B. Gutenberg and C. F. Richter, "Earthquake Magnitude, Intensity, Energy and Acceleration," Paper 2, Bull. Seism. Soc. Am. 40, 105 (1956).
24. R. B. Hofman, "Factors in the Specification of Ground Motions for Design Earthquakes in California," Misc. Paper 5-73-1, U. S. Army Engineer Waterways Experiment Station (Vicksburg, 1974).
25. G. W. Housner, "Intensity of Earthquake Ground Shaking Near the Causative Fault," Proc. 3rd World Conference on Earthquake Engineering 1 (New Zealand, 1965).

*Available for purchase from the NRC/GPO Sales Program, U.S. Nuclear Regulatory Commission, Washington, DC 20555, and/or the National Technical Information Service, Springfield, VA 22161.

26. R. A. Page, D. M. Boore, W. B. Joyner, and H. W. Coutler, Ground Motion Values for Use in the Seismic Design of the Trans-Alaska Pipeline System, U.S. Geological Survey Circular 672 (1972).
27. K. Kanai, "Improved Empirical Formula for the Characteristics of Strong Earthquake Motion," Proceedings, Japan Earthquake Symposium (Tokyo, Japan, 1966).
28. H. B. Seed, I. M. Idress, H. Bolton, and F. W. Kiefer, "Characteristics of Rock Motions During Earthquakes," Journal of Soil Mechanics and Foundations Division, Proceedings, American Society of Civil Engineers (1969).
29. P. B. Schnabel and H. B. Seed, "Acceleration in Rock for Earthquakes in the Western United States," Bull. Seism. Soc. Am., 63, 750 (1973).
30. P. B. Schnabel, J. Lysmer and H. B. Seed, SHAKE - A Computer Program for Earthquake Response Analysis of Horizontally Layered Sites, Earthquake Engineering Research Center, University of California, Berkeley, California, Report EERC-72-12 (1972).
31. H. B. Seed et al., "Relationships of Maximum Acceleration, Velocity, Distance from Source and Local Site Conditions for Moderately Strong Earthquakes," Bull. Seism. Soc. Am. 66, 1323-1324 (1976).
32. J. N. Brune, "Tectonic Stress and the Spectra of Seismic Shear Waves from Earthquakes," J. Geophys. Res. 75, 4997-5009 (1970).
33. D. Chung and D. L. Bernreuter, Regional Relationships Among Earthquake Magnitude Scales, Report UCR-2745, Lawrence Livermore National Laboratory, Livermore, California (1980).
34. N. N. Ambraseys, "The Correlation of Intensity with Ground Motions," in Advances in Engineering Seismology in Europe (Trieste, 1974).
35. H. J. Swanger, J. R. Murphy, T. J. Bennett, and R. Guzman, State-of-the-Art Study Concerning Near-Field Earthquake Ground Motion, Systems, Science and Software: Annual Technical Report to the Nuclear Regulatory Commission, SSS-R-80-4217 (1979).
36. J. H. Dieterich, "A Deterministic Near-Field Source Model," Proc. of 5th World Conf. on Earthquake Engineering, (Rome, 1973).
37. B. V. Kostrov, "Self-Similar Problems of Propagating Shear Cracks," J. Appl. Math. Mech. 28, 1077-1087 (1964).
38. B. V. Kostrov, "The Inverse Problem of the Theory of Earthquake Foci," Bull. (Izv.) Acad. Sci., USSR, Earth Physics 9 (1968).

39. R. Madariaga, "Dynamics of an Expanding Circular Fault, Bull. Seism. Soc. Am. 66, 639-666 (1976).
40. R. Madariaga, "High Frequency Radiation from Crack (Stress Drop) Models of Earthquake Faulting," Geophys. J. 51, 625-651 (1977).
41. R. Madariaga, "Implications of Stress-Drop Models for the Inversion of Stress Drop from Seismic Observations," Pure and Appl. Geophys. 115, 301-316 (1977).
42. R. Madariaga, "The Dynamic Field of Haskell's Rectangular Dislocation Fault Model," Bull. Seism. Soc. Am. 68, 869-887 (1978).
43. S. Das, A Numerical Study of Rupture Propagation and Earthquake Source Mechanism, Sc.D. Thesis, Massachusetts Institute of Technology, Cambridge, Massachusetts (1976).
44. S. Das and K. Aki, "A Numerical Study of Two-Dimensional Spontaneous Rupture Propagation," Geophys. J. 50, 643-668 (1977).
45. S. Das and K. Aki, "Fault Plane with Barriers: A Versatile Earthquake Model," J. Geophys. Res. 82, 5658-5670 (1977).
46. K. Aki, "Characterization of Barriers on an Earthquake Fault, J. Geophys. Res. 84, 6140-6148 (1979).
47. M. Wyss and J. N. Brune, "The Alaska Earthquake of 28 March 1964: A Complex Multiple Rupture", Bull. Seism. Soc. Am. 57, 1017-1023 (1967).
48. M. Trifunac and J. N. Brune, "Complexity of Energy Release During The Imperial Valley, California, Earthquake of 1940," Bull. Seism. Soc. Am. 60, 137-160 (1970).
49. K. Aki and B. Chouet, "Origin of Code Waves: Source, Attenuation, and Scattering Effects," J. Geophys. Res. 80, 3322-3342 (1975).
50. J. N. Brune, R. J. Archeleta, and S. Hartzell, "Far-Field S-Wave Spectra, Corner Frequencies and Pulse Shapes," J. Geophys. Res. 84, 2262-2272 (1979).
51. F. Sauer (Ed.), Nuclear Geophysics, DASA 1285 (1964).
52. K. Aki, "Scaling Law of Seismic Spectrum," J. Geophys. Res. 72, 1217-1231 (1967).
53. D. L. Bernreuter, E. C. Jackson, and A. B. Miller, "Control of the Dynamic Environment Produced by Underground Nuclear Explosives," Proc. Symp. on Engineering with Nuclear Explosives, USAEC Conf.-700101 2, 973-993 (Las Vegas, Nevada, 1970).
54. J. R. Murphy and J. A. Lahoud, "Analysis of Seismic Peak Amplitudes from Underground Nuclear Explosions," Bull. Seism. Soc. Am. 59 (1969).

55. Environmental Research Corp., Prediction of Ground Motion Characteristics of Underground Nuclear Detonations, AEC Report NVO-1163-239.
56. Environmental Research Corp., Observed Ground Motion Data Boxcar Event, AEC Report NVO-1163-155.
57. L. M. Lowrie and W. V. Mickey, Project Danny Boy, Seismic Effects from a Nuclear Cratering Experiment in Basalt, Report AEC WT-1813 (1965).
58. L. M. Lowrie and W. V. Mickey, Project Dugout, Strong-Motion Seismic Measurements, Coast and Geodetic Survey Report PNE-605F (1965).
59. R. W. Terhune, Project Dugout, Surface Motion Measurements, Oak Ridge National Laboratory, PNE-603F (December 1965).
60. Environment Research Corporation, Buggy, Analysis of Ground Motion, AEC Report PNE-326 (1969).
61. J. Toman, Project Buggy: A Nuclear Row Excavation Experiment, Lawrence Livermore National Laboratory, Livermore, California, UCRL-71280 (1968).
62. C. E. Joachim, Project Pre-Gondala II, Close-in Ground Motion and Earth Stress, U. S. Army Engineers Waterways Experiment Station, Vicksburg, Mississippi, PIVE 1113 (1968).
63. D. V. Power, Intermediate Range Ground Motions for Pre-Gondola II and Associated Events, Lawrence Livermore National Laboratory, Livermore, California, UCRL-504433 (1968).
64. D. R. Schlater, DIHEST Improvement Program Test, DIP IIA, Data Report, Air Force Weapons Laboratory AFWL-TR-72-35 (1972).
65. K. B. Simmons, Direct-Induced, High-Explosive Simulation Technique Improvement Program Tests (DIP IVA and DIPVA), Air Force Weapons Laboratory AFWL-TR-74-238 (1976).
66. M. D. Trifunac, "Stress Estimates for San Fernando, California Earthquake of Feb. 1971: Main Event and Thirteen Aftershocks," Bull. Seism. Soc. Am. 62, 721-750 (1972).
67. M. D. Trifunac, "Tectonic Stress and the Source Mechanism of the Imperial Valley Earthquake of 1940," Bull. Seism. Soc. Am. 62, 1283-1302 (1972).
68. Analysis of Strong Motion Earthquake Accelerograms IV, California Institute of Technology Earthquake Engineering Laboratory (1969-1975).
69. L. J. Burdick and G. R. Mellman, "Invasion of the Body Waves from the Borrego Mountain Earthquake to the Source Mechanism," Bull. Seism. Soc. Am. 66, 1485-1499 (1976).

70. T. H. Heaton and D. V. HelMBERGER, "A Study of the Strong Ground Motion of the Borrego Mountain, California Earthquake," Bull. Seism. Soc. Am. 67, 315-330 (1977).
71. D. M. Boore, W. B. Joyner, A. A. Oliver, and R. A. Paige, Estimation of Ground Motion Parameters, Geological Survey Circular 795 (1978).
72. J. Anderson, "A Dislocation Model for the Parkfield Earthquake," Bull. Seism. Soc. Am. 64, 671 (1974).
73. J. Shoja-Taheri, Seismological Studies of Strong Ground Motion Records, University of California, Berkeley, California, Earthquake Engineering Research Center Report UCB/EERC-77/04 (1977).
74. M. D. Trifunac and F. E. UdWADIA, "Parkfield, California Earthquake of June 27, 1966: A Three-Dimensional Moving Dislocation," Bull. Seism. Soc. Am. 64, 511-533 (1974).
75. T. C. Hanks, "The Faulting Mechanism of the San Fernando Earthquake," J. Geophys. Res. 79, 1215-1229 (1974).
76. M. Bouchon, "A Dynamic Source Model for the San Fernando Earthquake," Bull. Seism. Soc. Am. 68, 1555-1576 (1978).
77. T. C. Bache and T. G. Barker, The San Fernando Earthquake - A Model Consistent with Near-Field and Far-Field Observations at Long and Short Periods, Systems, Science and Software Final Technical Report submitted to the U.S. Geological Survey, SSS-R-79-3552 (1979).
78. R. L. Porcella and R. B. Matthiesen, Preliminary Summary of the U.S.G.S. Strong-Motion Records from the October 15, 1979 Imperial Valley Earthquake, U.S. Geological Survey Open-File Report 79-1654 (1979).
79. R. D. McJunkin and J. T. Ragsdale, Compilation of Strong-Motion Records from the August 6, 1979 Coyote Lake Earthquake, U.S. Geological Survey Report 79-385.
80. K. McNally, 1979 Calexico Earthquake: Seismological Data, EERI Reconnaissance Report, Imperial County, California Earthquake October 15, 1979, 21-31, 1980.
81. T. C. Hanks, "Strong Ground Motion of the San Fernando, California, Earthquake: Ground Displacements," Bull. Seism. Soc. Am. 65, 193-225 (1975).
82. W. Thatcher and T. C. Hanks, "Source Parameters of Southern California Earthquakes," J. Geophys. Res. 78, 8547-8576 (1973).
83. H. Kanazori and P.C. Jennings, "Determination of Local Magnitude, M_L , from Strong-Motion Accelerograms," Bull. Seism. Soc. Am. 68, 471-485 (1978).

NRC FORM 335 (7-77)		U.S. NUCLEAR REGULATORY COMMISSION BIBLIOGRAPHIC DATA SHEET		1. REPORT NUMBER (Assigned by DDCI) NUREG/CR-2103 UCRL-53020	
4. TITLE AND SUBTITLE (Add Volume No., if appropriate) Scaling and Estimation of Earthquake Ground Motion as a Function of the Earthquake Source Parameters and Distance				2. (Leave blank)	
7. AUTHOR(S) D. L. Bernreuter				3. RECIPIENT'S ACCESSION NO.	
9. PERFORMING ORGANIZATION NAME AND MAILING ADDRESS (Include Zip Code) Lawrence Livermore National Laboratory P.O. Box 808 Livermore, California 94550				5. DATE REPORT COMPLETED MONTH YEAR April 1981	
12. SPONSORING ORGANIZATION NAME AND MAILING ADDRESS (Include Zip Code) Office of Nuclear Regulatory Research U.S. Nuclear Regulatory Commission Washington, D. C. 20555				DATE REPORT ISSUED MONTH YEAR June 1981	
				6. (Leave blank)	
				8. (Leave blank)	
				10. PROJECT/TASK/WORK UNIT NO.	
				11. CONTRACT NO. FIN A0223	
13. TYPE OF REPORT Technical			PERIOD COVERED (Inclusive dates)		
15. SUPPLEMENTARY NOTES				14. (Leave blank)	
16. ABSTRACT (200 words or less) In this report we review the various methodologies currently available to predict the near-source ground motion from an earthquake. The limitations of the various approaches are discussed in light of recently developed theory and recorded data. To overcome some of the limitations of available approaches, we developed improved rules for scaling between earthquakes. Ground-motion data obtained from salvo (line source) explosions are also investigated to gain insight into the appropriate form for the attenuation of peak acceleration and peak velocity. The scaling laws are combined with the appropriate attenuation relations and the data from the 1971 San Fernando and 1940 Imperial Valley earthquakes to obtain relations among the key source parameters: dynamic stress drop and equivalent radius of the highly stressed region, distance from the center of energy release, and peak ground acceleration and velocity. These relations are verified by comparing the predicted levels of ground motion to those actually recorded from a number of earthquakes. The relations among earthquake magnitude, earthquake source parameters, and peak ground motion are discussed.					
17. KEY WORDS AND DOCUMENT ANALYSIS			17a. DESCRIPTORS		
17b. IDENTIFIERS/OPEN-ENDED TERMS					
18. AVAILABILITY STATEMENT UNLIMITED			19. SECURITY CLASS (This report) UNCLASSIFIED		21. NO. OF PAGES
			20. SECURITY CLASS (This page) UNCLASSIFIED		22. PRICE \$